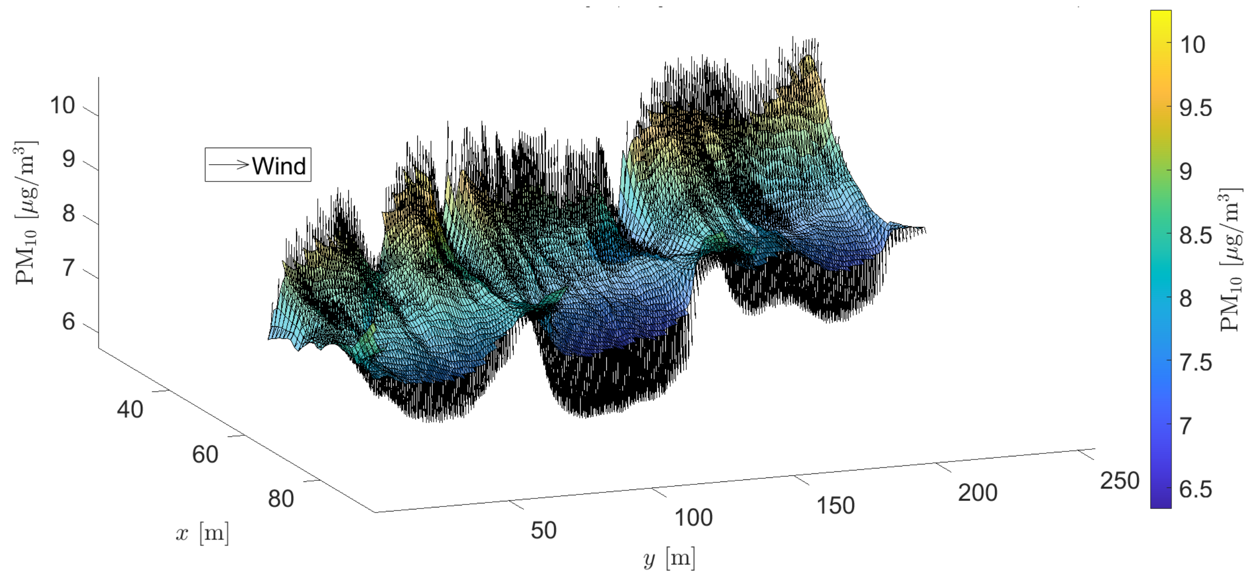

Correlation between pollution levels and city design

How different building and vegetation scenarios affect air pollution at Fabriksgatan, Gothenburg — for different wind configurations and emission scenarios

Master's thesis in Industrial Ecology

EMELIE JOHANSSON

MECHANICS AND MARITIME SCIENCES
Division of Fluid Dynamics

CHALMERS UNIVERSITY OF TECHNOLOGY
Gothenburg, Sweden 2022
www.chalmers.se

Master's thesis 2022

Correlation between pollution levels and city design

How different building and vegetation scenarios affect air pollution at Fabriksgatan, Gothenburg — for different wind configurations and emission scenarios

Emelie Johansson

Mechanics and Maritime Sciences
Division of Fluid Dynamics
Chalmers University of Technology
Gothenburg, Sweden 2022

Correlation between pollution levels and city design
How different building and vegetation scenarios affect air pollution at Fabriksgatan, Gothenburg — for different wind configurations and emission scenarios
EMELIE JOHANSSON

Supervisor: Malin Gustafsson, IVL
Examiner: Henrik Ström, Mechanics and Maritime Sciences

Master's Thesis 2022
Mechanics and Maritime Sciences
Division of Fluid Dynamics Chalmers University of Technology
SE-412 96 Gothenburg
Telephone +46 31 772 1000

Cover: Concentration of PM_{10} (in µg/m^3) and three-dimensional wind flow at $z = 10.5\,\text{m}$, which represents the canopy height for a row of trees. The row of trees consist of English oaks and is dense. The study area is Fabriksgatan in Gothenburg and the building scenario is S2, which consists of large houses with courtyards to the west of Fabriksgatan and elongated houses to the east of Fabriksgatan.

Typeset in LaTeX
Printed by Chalmers Digitaltryck
Gothenburg, Sweden 2022

Correlation between pollution levels and city design
How different building and vegetation scenarios affect air pollution at Fabriksgatan, Gothenburg — for different wind configurations and emission scenarios
Emelie Johansson
Mechanics and Maritime Sciences
Chalmers University of Technology

Abstract

Air pollution threat public health, the environment and objects of cultural value. It also affects the climate and is a big problem in many cities. It is therefore of interest to design cities in such a way that pollution levels are low. Pollution levels could be decreased via dispersion (when pollutants are diluted) and deposition (when pollutants deposit at surfaces).

This report study how shape and size of buildings and different vegetation scenarios (one with just background vegetation; one with a sparse row of English oaks and background vegetation; one with a dense row of English oaks and background vegetation; and one with a green wall made of ivy and background vegetation) affect pollution levels of NO, NO_2, O_3, PM_{10} and $PM_{2.5}$ for different wind configurations and emission scenarios for a specific area. The area is Fabriksgatan in Gothenburg and its surroundings. Two different street canyon widths are studied: one representing the width today and one wider, with room for a bike- and walkway and a row of trees. For this, the large eddy simulation (LES) model PALM, based on Fortran-code, is used.

The main findings are that a wide street canyon enables more circulation and thus lower pollution levels. Small point houses open up the street canyon and such configurations have lower pollution levels than more confined street canyons. Both buildings and vegetation could be used to shield out emissions, but vegetation generally increases mean concentrations. This is believed to be due to an incomplete implementation of the effects of deposition in PALM. Thus, the effects of deposition must be studied in more detail before general advice on vegetation could be made.

Keywords: Air pollution, urban vegetation, city design, large eddy simulation, PALM

Acknowledgements

First of all, I want to thank my supervisor Malin Gustafsson for her help and support, and IVL for providing me the opportunity to do this thesis. I also want to thank Jenny Lindén, David Rayner and Fredrik Lindberg for discussions and their insights.

The computations were enabled by resources provided by the Swedish National Infrastructure for Computing (SNIC), partially funded by the Swedish Research Council through grant agreement no. 2018-05973. Without that, this thesis would have been impossible to do.

I also want to thank the Copernicus Atmosphere Monitoring Service (CAMS) Atmosphere Data Store (ADS) (`https://ads.atmosphere.copernicus.eu/cdsapp#!/dataset/cams-global-reanalysis-eac4?tab=overview`) for providing data used to obtain height distributions of background data for different pollutants.

Last but not least, thanks to Viktor for your proofreading, support and LaTeX skills.

Emelie Johansson, Gothenburg, December 2021

Contents

List of Figures

List of Tables

Chapter 1

Introduction

One big threat to public health is air pollution, causing for example cardio-vascular and respiratory diseases which claims over 4 million premature deaths globally every year (Cai, Xin, and Yu, 2017; World Health Organization, 2018). Furthermore, air pollution can affect the climate, the environment as well as causing acid rain, which can harm buildings, statues and other objects of cultural value (Eljarrat et al., 2020). It is therefore essential to decrease air pollution.

The concentration of air pollutants could be decreased via dispersion and deposition. Dispersion occurs when particles and molecules are diluted in the air, which reduces the concentration of pollutants. Deposition occurs when particles and molecules pass near a surface and deposit at that surface, and the chance for deposition increases with a high surface area (Janhäll, 2015). Note that dispersion reduces only the concentration of pollutants, not the amount, while deposition reduces both.

The most obvious way to decrease air pollution is to decrease the sources of pollutants. However, how to achieve that will have to be the subject for another thesis, since this thesis focuses on mechanisms that reduces the concentration of pollutants. This work is a part of the project CityAirSim, which investigates how the air in cities is affected by traffic, buildings and vegetation (Mistra Urban Futures, n.d.).

One possible way to decrease air pollution could be to use more vegetation in cities (Janhäll, 2015). Here one important factor is the height of the vegetation. With high vegetation, e.g. trees, the circulation with clean air above the ground could be limited, which in fact could worsen the air pollution since the dilution decreases (Abhijith et al., 2017). With lower vegetation, e.g. hedges, the circulation is not hindered. Another advantage with low vegetation is that it is often closer to the source (for example the exhaust pipe of a car), meaning that it is where the pollution concentration is at maximum. According to Janhäll (2015), the deposition is higher when the pollution concentration is higher, leading to a more efficient reduction of air pollution levels in those cases. Vegetation could also increase air pollution by re-suspension of previously deposited particles or by wash-off, when deposited particles are washed off due to rainfall.

Even the shape and size of buildings will affect the pollution levels. In for example a street canyon, the circulation is limited, while it is larger in an open street. Trees could, as mentioned earlier, impair the air quality. Thus, in the case with a street canyon (with an already low circulation), there could be reasons to not have any trees (Abhijith et al., 2017). In an open road, a wall (made of building material or vegetation) could be used as a barrier between for example cars and pedestrians. The wall could then decrease the dispersion to the pedestrian's area, acting as a shield. However, the wall could also increase the pollution concentration just behind the wall, due to turbulence.

In a study by Aristodemou et al. (2018), it was shown that if high buildings surround the pollution source, the pollution concentration increases near the source. But it could also be seen that higher buildings close to the source improve the air quality downwind. A more varied height distribution of buildings in a city may increase the turbulence and thereby the circulation (Carpentieri and Robins, 2015).

Walls, or barriers, could also be used to filter the air, if they are porous (Janhäll, 2015). If they are too porous, all air (and thus all air pollution) will just move through them and if they are not porous at all, they will just act as a solid wall (Abhijith et al., 2017).

Chapter 2

Theoretical background

In this section, the theoretical model for air pollutants and the computational model for the fluid dynamics are presented. Furthermore, the aim and connected research questions are stated.

2.1 Air pollutants

Air pollution could be from both anthropogenic and natural sources. Example of anthropogenic sources are industries, household heating and cars, and one example of a natural source are forest fires (Eljarrat et al., 2020). Some sources are stationary, as an industry, and only pollutes in one place, while others are mobile, like cars, and could pollute many places. Common air pollutants are gases like ozone (O_3), nitric oxide (NO), nitrogen dioxide (NO_2) - NO and NO_2 are together called NOx - and carbon monoxide (CO), and particulate matter (PM) (Jacobsson, 2012). A pollutant is a primary pollutant if it is emitted directly from the source and a secondary pollutant if it is formed from a primary pollutant.

O_3 occurs naturally in the stratosphere, protecting life on Earth from harmful ultraviolet radiation, but closer to the ground, in the troposphere, it is a pollutant. There are no emissions of O_3, instead it is a secondary pollutant, formed from other primary pollutants. Exposure to O_3 could cause breathing problems and respiratory diseases (World Health Organization, 2021a). O_3 also has effects on the respiratory system and affects the forest and crops in a negative way (Naturvårdsverket, 2020a). It is also a greenhouse gas in the troposphere and it thus contributes to global warming both as a direct greenhouse gas and indirect since it degrade forest and crops, which in turn will store less carbon dioxide (CO_2) (Naturvårdsverket, 2020a). NO and NO_2 comes mainly from combustion of fossil fuels, from transportation and industry (Jacobsson, 2012). NO has no harmful effects on humans at typical concentrations in air, but it is involved in the reactions between NO_2 and O_3, which have effects on human health. NO_2 has large health effects on the respiratory system and the cardiovascular system (World Health Organization, 2021a).

The reactions of NO, NO_2 and O_3 are given by the following set of equations (Jacobsson, 2012):

$$NO + O_3 \rightarrow NO_2 + O_2, \tag{2.1}$$
$$NO_2 + h\nu \rightarrow NO + O, \tag{2.2}$$
$$O + O_2 \rightarrow O_3, \tag{2.3}$$

where $h\nu$ is energy from incoming solar light. Since there is no incoming light at night, the reaction described in equation (2.2) will not take place during nighttime. This will lead to a halt in the production of NO and O, which will reduce the production of O_3 in equation (2.3) (since that reaction involves O). Even if there is no production of NO during nighttime, there will still be emissions (but much lower than during daytime) of NO (and remnants from the day). Thus, the reaction described in equation (2.1) will continue, causing a destruction of O_3 (Jacobsson, 2012).

Volatile organic compounds, which originates from example incomplete combustion of fossil fuels can react with NO and form NO_2. With lower levels of NO, the reaction described in equation (2.1) will slow down, decreasing the destruction of O_3. The after all formed NO_2 can react and in turn form more O_3 (Jacobsson, 2012). There are also natural sources of volatile organic compounds, for example isoprene emitted by trees (European Commission, 2010).

CO comes from incomplete combustion of fossil fuels (Eljarrat et al., 2020). CO decreases the amount of oxygen transported in the bloodstream, making it potentially fatal in high concentrations. It is mainly a problem indoors but sometimes pollution levels are high outdoors as well (World Health Organization, 2021a).

Particulate matter originates for example from combustion of fossil fuels, industrial activities (World Health Organization, 2021a), and also from transportation via tyre wear. Particulate matter consists of for example black carbon, sulphate, nitrate, but also water (World Health Organization, 2021a). The particulate matter could be emitted directly, or be formed in the atmosphere after emissions of for example sulfur dioxide (SO_2), NO and NO_2 (Hassan et al., 2020). Particulate matter is divided into PM_{10}, which have a size of $\leq 10\,\mu m$, and $PM_{2.5}$, which have a size of $\leq 2.5\,\mu m$, meaning that $PM_{2.5}$ is included in PM_{10}. Particulate matter could also be divided into ultrafine particles, with a size of $\leq 0.1\,\mu m$ (Hassan et al., 2020), but they are not included in this study. The particles could pass the lungs and enter the bloodstream, and this risk is larger for smaller particles (Eljarrat et al., 2020). Exposure to particulate matter is linked to a range of negative health effects, such as cardiovascular diseases (Eljarrat et al., 2020).

The Swedish Environmental Protection Agency (EPA) has 16 environmental objectives, where one is about clean air. In this goal, limits for pollutants are given. The World Health Organisation (WHO) also have guidelines (which were updated 2021). Both will be presented in table 2.1, where values for NO_2, O_3, PM_{10} and $PM_{2.5}$ are given.

Air pollution also affect climate change. Some particulate matter, e.g. black carbon, absorbs solar radiation, and thus contribute to global warming, while others, e.g. SO_2, reflect light, thus having a cooling effect (Arneth et al., 2009). Air pollutants are in general short-lived, which means that in the short-term, a reduction of

Table 2.1: *Limits and guidelines for NO_2, O_3, PM_{10} and $PM_{2.5}$ from the Swedish EPA (Naturvårdsverket, 2020b) and WHO (World Health Organization, 2021b).*

	Swedish EPA	WHO
NO_2 [ppm]	0.03137 (hourly mean)	0.01307 (daily mean)
O_3 [ppm]	0.04009 (hourly mean)	0.05012 (8-hour mean)
PM_{10} [µg/m^3]	30 (daily mean)	45 (daily mean)
$PM_{2.5}$ [µg/m^3]	25 (daily mean)	15 (daily mean)

air pollution could increase the temperature. In the long-term, longer-lived species (such as CO_2), will dominate (European Commission, 2010).

Some air pollutants are also greenhouse gases, for example ground-level O_3. European Commission (2010) suggests that a warmer climate will increase the amount of emitted isoprene, which will increase the pollution levels of O_3. They also suggest that the deposition of O_3 on plants will decrease in a drier climate, causing a positive feedback loop for O_3.

Temperature and weather also affect air pollution levels. Usually, air temperature decreases with height in the troposphere, but when the surface is cold and the wind is calm, the air close to the ground is cooled down. This results in a warmer air parcel above, acting as a lid. This is called inversion and prevents the air from mixing and thus decreases the dispersion, which in turn increases the pollutant concentration (Samad et al., 2020). When it is sunny and warm, air close to the ground is heated and thus rises in the atmosphere. The colder air higher in the troposphere will then sink, and this will result in a circulation that move air pollutants close to the surface higher up in the atmosphere. This is called convection and reduces the concentration of air pollutants (UCAR Center for Science Education, 2020).

Vegetation will also affect air pollution levels, not only with deposition, but also with changed circulation. The viscous drag forces due to vegetation will reduce the flow. The reduction will depend on wind velocity and the shape and size of the vegetation (Kurppa, Hellsten, et al., 2018). The plant canopy will be a sink for momentum (because of form drag forces and viscous drag forces) and a sink or source for scalars (PALM group, 2015). The drag forces are larger for sturdy trees and smaller for more flexible trees, which usually are younger or smaller trees. The deposition velocity (defined as the ratio of the dry deposition flux and the pollutant concentration (Giardina and Buffa, 2018)) will vary among pollutants (Buccolieri et al., 2019). Vegetation usually affect air quality more because of different turbulence patterns than because of deposition (Buccolieri et al., 2019).

Vegetation also affect the temperature, which will affect the turbulence and thus the pollution levels (Buccolieri et al., 2019). When the temperature is low, inversion is more likely to happen.

2.2 PALM

For this project, the model system PALM will be used, see first description in Raasch and Schröter (2001) and most recent description in Björn Maronga et al.

(2020). PALM is a large eddy simulation (LES) model used in computational fluid dynamics (Karttunen et al., 2020). In a LES model, large eddies are resolved by the grid and since the grid needs to be very fine to resolve small eddies (and thus making the computation very expensive), a subgrid scale (SGS) model is used for the small eddies (Fluid Mechanics 101, 2020). A filter is applied to filter out small turbulence and the eddies that are not filtered out are resolved by the LES model. The eddies that are filtered out are parameterised in a SGS model (Björn Maronga et al., 2020). Around 90% of the turbulent kinetic energy can be resolved with PALM (B. Maronga et al., 2015).

PALM solves Navier-Stokes equations that are assumed to not be in hydrostatic equilibrium. The equations are also filtered to get the larger eddies and will be solved using the Boussinesq-approximation (Karttunen et al., 2020). The Boussinesq-approximation means that the fluid is assumed to be incompressible and the density is assumed to be constant, except in the gravitational term. In that term, the density is assumed to depend linearly on the temperature difference (Tritton, 1977).

This leads to the following set of equations (Björn Maronga et al., 2020), where an overbar means that it is filtered and a prime means that it is a SGS variable:

$$\begin{aligned}
\frac{\partial \overline{u}_j}{\partial x_j} &= 0, \qquad (2.4)\\
\frac{\partial \overline{u}_i}{\partial t} &= -\frac{\partial \overline{u}_i \overline{u}_j}{\partial x_j} - \varepsilon_{ijk} f_j \overline{u}_k + \varepsilon_{i3j} f_3 u_{g,j} - \frac{1}{\rho_0}\frac{\partial \pi^*}{\partial x_i}\\
&\quad + g\frac{\overline{\theta}_v - \theta_{v,\mathrm{ref}}}{\theta_{v,\mathrm{ref}}}\delta_{i3} - \frac{\partial}{\partial x_j}\left(\overline{u_i'' u_j''} - \frac{2}{3}e\delta_{ij}\right), \qquad (2.5)\\
\frac{\partial \overline{\theta}}{\partial t} &= -\frac{\partial \overline{u}_j \overline{\theta}}{\partial x_j} - \frac{\partial}{\partial x_j}\left(\overline{u_j'' \theta''}\right) - \frac{l_v}{c_p \Pi}\Psi_{q_v}, \qquad (2.6)\\
\frac{\partial \overline{q}_v}{\partial t} &= -\frac{\partial \overline{u}_j \overline{q}_v}{\partial x_j} - \frac{\partial}{\partial x_j}\left(\overline{u_j'' q_v''}\right) + \Psi_{q_v}, \qquad (2.7)\\
\frac{\partial \overline{s}}{\partial t} &= -\frac{\partial \overline{u}_j \overline{s}}{\partial x_j} - \frac{\partial}{\partial x_j}\left(\overline{u_j'' s''}\right) + \Psi_s, \qquad (2.8)
\end{aligned}$$

where equation (2.4) is conservation of mass, equation (2.5) is conservation of momentum, equation (2.6) is conservation of thermal energy, equation (2.7) is conservation of moisture and equation (2.8) is conservation of a passive scalar. The indices i, j, k can take the values $1, 2, 3$ and u_i is the velocity, with $u_1 = u, u_2 = v, u_3 = w$. x_i is the location, with $x_1 = x, x_2 = y, x_3 = z$ and t is time. ε_{ijk} is the Levi-Civita tensor, $f_i = (0, 2\Omega\cos\phi, 2\Omega\sin\phi)$ is the Coriolis parameter with the angular velocity of the Earth as $\Omega = 0.729 \cdot 10^{-4}\,\mathrm{rad/s}$ and ϕ is the latitude. $u_{g,j}$ is the component of the geostrophic wind speed, ρ_0 is the density of dry air and $\pi^* = p^* + \frac{2}{3}e\rho_0$ is the modified perturbation pressure, where p^* is the perturbation pressure and $e = \frac{1}{2}\overline{u_i'' u_i''}$ is the SGS turbulence kinetic energy. $g = 9.81\,\mathrm{m/s^2}$ is the gravitational acceleration, θ_v is the virtual potential temperature and $\theta_{v,\mathrm{ref}}$ is a reference state for the virtual potential temperature (the definition will be presented after the definition of potential temperature). It could be seen that the temperature difference is included in the gravity term in the equation for conservation of momentum (equation (2.5)), which arises from the Boussinesq approximation described above. δ is the Kronecker delta and θ is the potential temperature, given by $\theta = \frac{T}{\Pi}$, where T is the absolute temperature and $\Pi = \left(\frac{p}{p_0}\right)^{R_d/c_p}$ is the Exner function. p is the hydrostatic air pressure, $p_0 = 1000\,\mathrm{hPa}$ is a reference pressure, $R_d = 287\,\mathrm{J/(kg \cdot K)}$ is the specific gas constant for dry air and $c_p = 1005\,\mathrm{J/(kg \cdot K)}$ is the specific heat of dry air (at constant pressure). By this, the virtual potential temperature is defined as $\theta_v = \theta\left(1 + \left(\frac{R_v}{R_d} - 1\right) q_v - q_l\right)$. $R_v = 461.51\,\mathrm{J/(kg \cdot K)}$ is the specific gas constant for water vapor, q_v is water vapor mixing ratio and q_l is liquid water mixing ratio. $l_v = 2.5 \cdot 10^6\,\mathrm{J/kg}$ is the specific latent heat of evaporation, Ψ_{q_v} is the sink/source term of q_v, s is a passive scalar and Ψ_s is the sink/source term of s (Björn Maronga et al., 2020).

The SGS terms are parameterised in the following way:

$$
\begin{aligned}
\overline{u_i'' u_j''} - \frac{2}{3} e \delta_{ij} &= -K_m \left(\frac{\partial \overline{u}_i}{\partial x_j} + \frac{\partial \overline{u}_j}{\partial x_i} \right), \\
\overline{u_i'' \theta''} &= -K_h \frac{\partial \overline{\theta}}{\partial x_i}, \\
\overline{u_i'' q_v''} &= -K_h \frac{\partial \overline{q}_v}{\partial x_i}, \\
\overline{u_i'' s''} &= -K_h \frac{\partial \overline{s}}{\partial x_i},
\end{aligned}
$$

where K_m is the local SGS eddy diffusivity of momentum and K_h is the local SGS eddy diffusivity of heat (B. Maronga et al., 2015). They are defined as

$$
\begin{aligned}
K_m &= 0.1 l \sqrt{e}, \\
K_h &= \left(1 + \frac{2l}{\boldsymbol{\Delta}}\right) K_m,
\end{aligned}
$$

where $\boldsymbol{\Delta} = \sqrt[3]{\Delta x \Delta y \Delta z}$, where Δx is the grid spacing in the x-direction, Δy is the grid spacing in the y-direction and Δz is the grid spacing in the z-direction. l is the SGS mixing length and depends on z, $\boldsymbol{\Delta}$ and the stratification. The SGS mixing length l is calculated as in B. Maronga et al. (2015), that is

$$
l = \begin{cases} \min\left(1.8z, \boldsymbol{\Delta}, 0.76\sqrt{e}\left(\frac{g}{\theta_{v,\mathrm{ref}}} \frac{\partial \overline{\theta}_v}{\partial z}\right)^{-\frac{1}{2}}\right) & \text{for } \frac{\partial \overline{\theta}_v}{\partial z} > 0, \\ \min\left(1.8z, \boldsymbol{\Delta}\right) & \text{for } \frac{\partial \overline{\theta}_v}{\partial z} \leq 0. \end{cases}
$$

With these equations, seven prognostic variables could be solved for: the velocities u, v, w, the potential temperature θ, the SGS turbulence kinetic energy e, the water vapor mixing ratio q_v and a passive scalar s. In these simulations, equation (2.8) will not be used since no passive scalar is studied. Instead, five extra prognostic equations (one for each pollutant) will be solved as well. These will be described later on.

2.3 Models in PALM that will be used

PALM has some embedded models that are useful for different applications. Those used for this project will be described in the following sections.

2.3.1 Land surface model

The land surface model consists of a liquid water reservoir, a soil model (for prediction of soil temperature and soil moisture) and an energy balance solver (PALM group, 2021b). The equation used for the energy balance solver is

$$C_0 \frac{\mathrm{d}T_0}{\mathrm{d}t} = R_n - H - LE - G, \tag{2.9}$$

where C_0 is the heat capacity of the surface skin layer, T_0 is the radiative temperature of the same layer, R_n is the net radiation, H is the sensible heat flux, LE is the latent heat flux and G is the soil heat flux (at the surface).

2.3.2 Radiation model

The radiation model will be used for clear sky, meaning no clouds and parameterised radiation fluxes (PALM group, 2021e). The net radiation R_n is calculated as

$$R_n = SW_{\text{in}} - SW_{\text{out}} + LW_{\text{in}} - LW_{\text{out}},$$

where SW_{in} is incoming shortwave radiation, SW_{out} is outgoing shortwave radiation, LW_{in} is outgoing longwave radiation and LW_{out} is outgoing longwave radiation. SW_{in} is given by $SW_{\text{in}} = S_0\,(0.6 + 0.2\cos\Psi)\cos\Psi$, where $S_0 = 1368\,\mathrm{W/m^2}$ is the solar constant. The expression between the parenthesis is atmospheric transmissivity and Ψ is the zenith angle, which depend on day of the year, time, longitude and latitude (PALM group, 2021e). SW_{out} is given by $SW_{\text{out}} = \alpha SW_{\text{in}}$, where α is the surface albedo. The incoming longwave radiation is given by $LW_{\text{in}} = \varepsilon_{\text{atm}}\sigma T_1^4$, where $\varepsilon_{\text{atm}} = 0.8$ is the emissivity of the atmosphere, $\sigma = 5.67 \cdot 10^{-8}\,\mathrm{W/(m^2K^4)}$ is the Stefan-Boltzmann constant and T_1 is the temperature at the first grid level. The outgoing longwave radiation is given by $LW_{\text{out}} = \varepsilon\sigma T_0^4$, where ε is the surface emissivity and T_0 is the temperature from equation (2.9).

2.3.3 Plant canopy model

The plant canopy model enables studies of the effect of plant canopy on the turbulence. The canopy drag coefficient is interesting for calculating the drag force. This coefficient will vary with tree and wind, but is typically around 0.20 (Cescatti and Marcolla, 2004), which is the value that will be used for these simulations.

The plant canopy is accounted for in PALM by adding a term to the conservation of momentum equation (equation (2.5)). The term is $-c_d \mathrm{LAD}\sqrt{\overline{u}_i^2}\,\overline{u}_i$, where c_d is the drag coefficient and LAD is the leaf area density (PALM group, 2015). Leaf area density is the total leaf area (for one side) per unit volume, meaning that the unit is $\mathrm{m^2/m^3}$ (Klingberg et al., 2017). The leaf area density will affect the turbulence, the canopy will act as a larger momentum sink for larger values of the leaf area density (PALM group, 2015). In Gothenburg is lime the most common tree (Klingberg et al., 2017), which has a leaf area density of around 0.67 m^2/m^3 (Klingberg et al., 2017).

The leaf area density is related to the leaf area index (LAI), which is the total leaf area (for one side) per unit area (for the ground surface), making it dimensionless (Klingberg et al., 2017). If the leaf area density is assumed to be constant through the canopy (as in Santiago, Martilli, and Martin (2017)), the relation is LAD = LAI/h, where h is the height of the vegetation. h could also be the thickness if the vegetation consists of a green wall (on for example a facade). This way, leaf area density does not change with height.

2.3.4 Urban surface model

The urban surface model consists of an energy balance solver, see equation (2.9), but it takes buildings into account as well (PALM group, 2021h).

2.3.5 Chemistry model

The chemistry model uses traffic emissions with different levels of detail (LOD). In these simulations, LOD0 will be used, meaning that emissions from traffic are separated for main streets and side streets. An emission value is given in micromole/(m^2·day) for gases and in kg/(m^2·day) for particulate matter, and this value is then multiplied with a factor for main streets, and another factor for side streets (PALM group, 2021a). Deposition of dry gases and particulate matter is allowed for horizontal surfaces, meaning that there will be deposition on vegetation at the ground, but not on trees (Khan et al., 2020). Photolysis is allowed, meaning that the incoming radiation could break down molecules and a simple photolysis scheme is used, taking the solar zenith angle into account (PALM group, 2021a).

The used chemical mechanism is an updated version of PALM's 'phstatp'. 'phstatp' includes NO, NO_2, O_3 and PM_{10}. In the updated version, $PM_{2.5}$ is also included. Thus, five pollutants will be studied, and for each of these pollutants, a three-dimensional prognostic equation on the following form will be solved (as before, an overbar will indicate that the variable is filtered and a prime means that it is a SGS variable):

$$\frac{\partial \overline{c}_n}{\partial t} = -\frac{\partial \overline{u}_i \overline{c}_n}{\partial x_i} - \frac{\partial}{\partial x_i}\left(\overline{u_i'' c_n''}\right) + \left(\frac{\partial \overline{c}_n}{\partial t}\right)_{\text{chem}} + \Psi_n, \tag{2.10}$$

where c_n is the concentration of pollutant n, u_i is the velocity, x_i is the position, Ψ_n are sources (emissions) and sinks (deposition) and $\left(\frac{\partial \overline{c}_n}{\partial t}\right)_{\text{chem}}$ is the change over time due to chemical reactions (Khan et al., 2020). This mechanism uses the following set of reactions:

$$NO_2 + h\nu \rightarrow NO + O_3, \tag{2.11}$$
$$NO + O_3 \rightarrow NO_2 + O_2, \tag{2.12}$$
$$PM_{10} \rightarrow PM_{10}, \tag{2.13}$$
$$PM_{2.5} \rightarrow PM_{2.5}, \tag{2.14}$$

where equation (2.11) and equation (2.12) are an amalgamation of equation (2.1), equation (2.2) and equation (2.3). Equation (2.13) and equation (2.14) shows reactions for the passive tracers (so they do not have any reactions).

2.4 Aim

Due to the previously described conditions and obstacles, it is of great interest to understand in detail how the shape and size of buildings affect pollution levels in different emission and wind conditions. The effect of kind and size of vegetation on pollution levels is also of interest. This will be the aim of this project. This knowledge could then be used in order to combat health hazards, climate change, environmental degradation and cultural loss.

2.5 Research questions

The aim is divided into the following research questions:

1. How will building size and shape affect the air quality in the study area?
2. How will street canyon width affect the air quality in the study area?
3. How will wind speed affect the air quality in the study area? Compare 1.0 m/s, 2.5 m/s and 5.0 m/s. How will wind direction affect air quality in the study area? Compare west and east wind.
4. How will emission scenarios affect pollution levels? Today vs. 10% more traffic but half of the vehicles are electric vehicles vs. 10% less traffic vs. same traffic volume but 50% electric vehicles (EV's).
5. Could houses be used to block emissions?
6. How will vegetation, and in particular a row of trees affect air pollution levels? Is there any difference between a dense and a sparse row of trees?
7. How will green walls affect air quality?

Chapter 3

Method

Large Eddy Simulation, which is a technique within Computational Fluid Dynamics, will be used for this work. More specifically, the model PALM will be used (described earlier). Matlab will be used for data analysis.

At first, an existing model for buildings will be studied in order to learn PALM. After that, a larger and more advanced model will be implemented, consisting of an inner and an outer domain. The area covered by the simpler, existing model will be the same as in the inner domain in the larger model. In this advanced model, vegetation, as well as other land use categories will be taken into account. Dry deposition on horizontal surfaces and radiation will be considered.

3.1 Demarcations

For the air pollution, focus will be on the pollutants NO, NO_2, O_3, particulate matter smaller than 10 µm (PM_{10}) and particulate matter smaller than 2.5 µm ($PM_{2.5}$) (but $PM_{2.5}$ will not be included for the simple model). The study area will be the street Fabriksgatan in Gothenburg, and its surrounding environment. The particular day studied will be June 28, 2019, and the time will be between 10.00 am and 12.00 pm. A summer day is chosen to have leaves on vegetation and this day is chosen since it was a sunny day with a temperature around 23 °C between 10.00 am and 12.00 pm (SMHI, n.d.[b]). With these weather conditions, the risk of inversion is decreased (UCAR Center for Science Education, 2020). The particular day was also a Friday, meaning that traffic conditions was as in a normal workday. Only emissions from traffic will be considered, e.g. emissions from domestic heating will not be considered. Since the simulated day will be in the middle of the summer, emissions from domestic heating will be negligible.

As mentioned, the project will start with a simpler model setup using no vegetation, one wind scenario (2.5 m/s west wind) and one emission scenario to look at the effects of buildings, before the more advanced model is implemented.

3.2 Description of the environment

The following two sections will describe the inner and outer domain. The details will be more described in section 3.5.

3.2.1 Inner domain

The inner domain is centered around a motorway. To the left of the motorway, there are building blocks with residential houses and offices around a street called Fabriksgatan, which is the focus area. To the left is also a stream, Mölndalsån, and not especially much vegetation. To the right of the motorway, the buildings consist mainly of individual houses. There is a significant amount of vegetation in this area, mainly deciduous trees, but also grass and to some extent also evergreen trees (S. Johansson, 2018). The map of the inner domain is shown in figure 3.1.

Figure 3.1: *A map of the inner domain, from OpenStreetMap contributors (2021).*

3.2.2 Outer domain

The outer domain is most extended to the left and right of the inner domain, but also below and above. The area to the left of the inner domain contains mainly of residential buildings and office buildings. There is some vegetation (mainly deciduous trees) and also some areas with bare soil. There are many streets, some with much traffic, as Skånegatan, Södra vägen and Örgrytevägen. To the right of the inner domain, the environment looks roughly the same as in the right part of the inner domain, with mainly individual houses and much vegetation (mainly deciduous trees but also grass and evergreen trees). The roads Danska vägen and Delsjövägen are highly trafficked. And the motorway is of course also highly trafficked. There are also two streams, Delsjöbäcken and Mölndalsån. The area above and below the inner domain looks roughly the same as the inner domain, with building blocks with residential and office buildings to the left of the motorway and smaller houses and more vegetation to the right of the motorway (S. Johansson, 2018). The map of the outer domain is shown in figure 3.2.

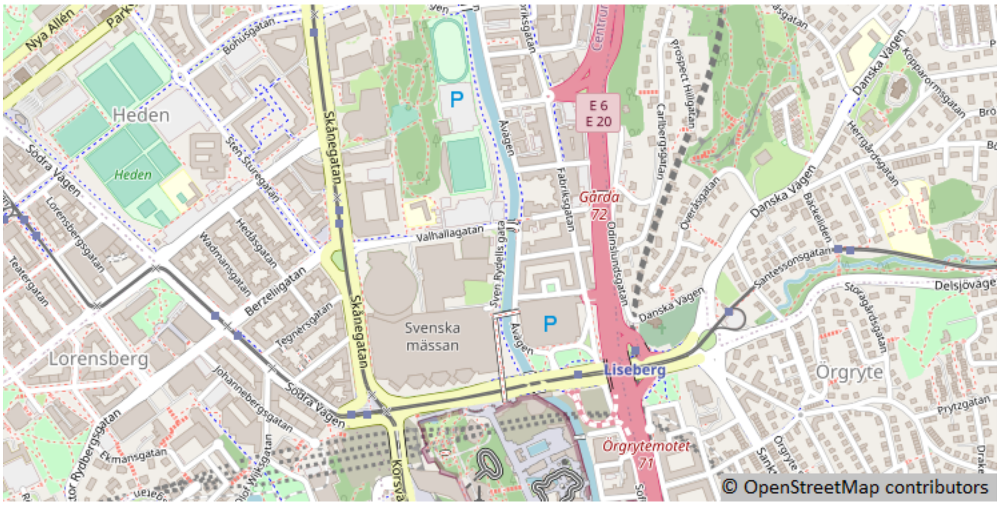

Figure 3.2: *A map of the outer domain, from OpenStreetMap contributors (2021).*

3.3 Topography and land use data

Light Detection and Ranging (LiDAR) data will be used as input to the model. This type of data is obtained by sending out infrared laser pulses from an airplane and register their reflections (returns) to the airplane (Lindberg, L. Johansson, and Thorsson, 2013). Since a pulse could be reflected several times (for example if it hits a tree), one laser pulse could give rise to several returns. The first return represents the highest elevation at that point, for example a treetop or the top of a building, and the last return represents the ground. If there are no buildings or vegetation, there will only be one return. Vegetation often give rise to multiple and complex returns, which could be used to distinguish vegetation from other surfaces.

The first returns are gathered in a Digital Surface Model (DSM) file and the last returns in a Digital Elevation Model (DEM) file. The returns from vegetation are collected into a Canopy Digital Surface Model (CDSM) file. The DEM file is used to obtain the terrain height for the domain and by subtracting the DEM file from the DSM file, the building heights are obtained. The vegetation height from the CDSM file is used to specify the vegetation. The CDSM file, the DSM file and the DEM file are obtained from Lindberg, L. Johansson, and Thorsson (2013).

A landcover file is obtained from S. Johansson (2018) where the land is divided into pavement, buildings, evergreen trees, deciduous trees, grass, bare soil and water. This file is used to implement the input file of the area to PALM.

3.4 Description of simple model

For the simple model, four different building scenarios will be studied, named *S0*, *S1*, *S2* and *S3*, where the buildings will be changed within the area of interest. The area of interest includes six blocks, three on each side of Fabriksgatan and the buildings will be represented by two dimensions, x and y. S0 represents the area today and is shown in figure 3.3, where the red rectangle represents the area of interest. It is in this area the houses will change among the scenarios. In this scenario, the main houses in the area of interest are between 10 m and 15 m high, with some a bit shorter and some a bit higher.

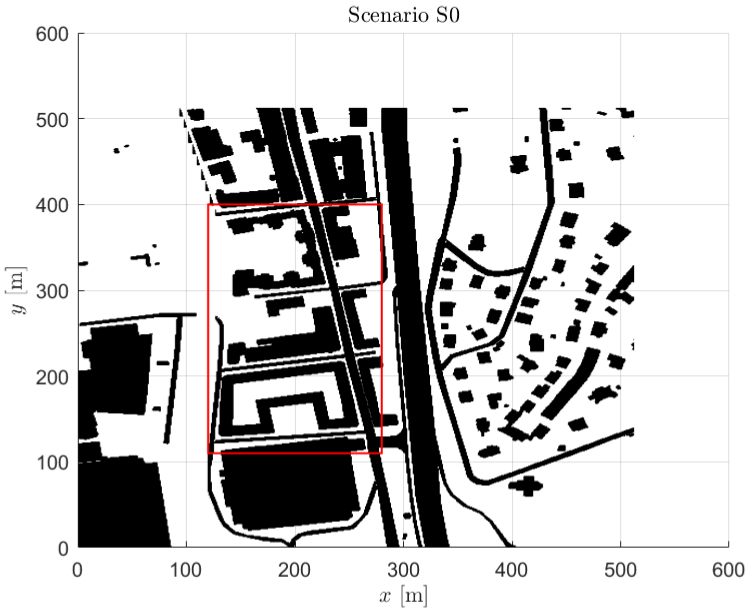

Figure 3.3: *Scenario S0, the red rectangle represents the area of interest.*

In S1, the houses in the area of interest are smaller but taller (between 20 m and 30 m) and more evenly distributed. The houses have no courtyards. The street canyon is wider, to make room for vegetation and a bike- and walkway. The scenario is shown in figure 3.4 and the red rectangle represents the area of interest.

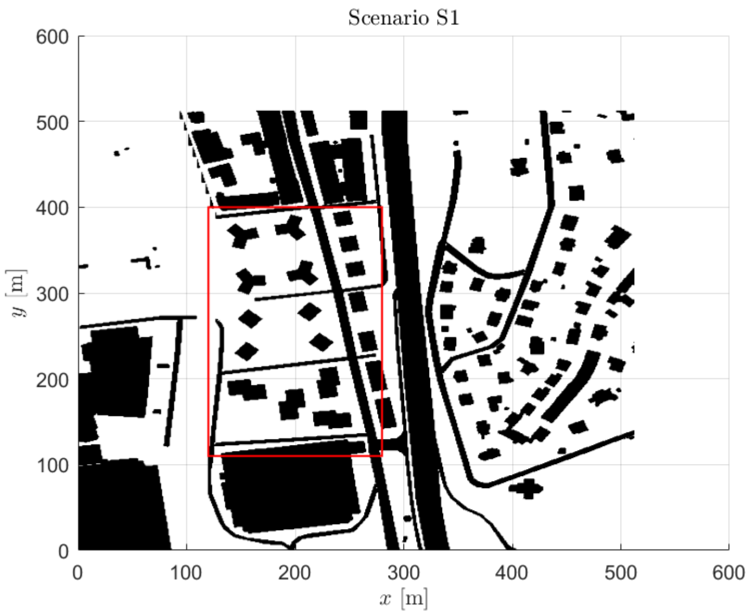

Figure 3.4: *Scenario S1, the red rectangle represents the area of interest.*

In S2, the houses are larger than in S1, and the three houses to the west of Fabriksgatan have large courtyards and are between 20 m and 25 m high, with the middle house being a bit shorter. At the other side of the street, the houses are long and narrow and around 25 m high. They almost form a wall against the highway. The scenario also has a wider street canyon. The scenario is shown in figure 3.5.

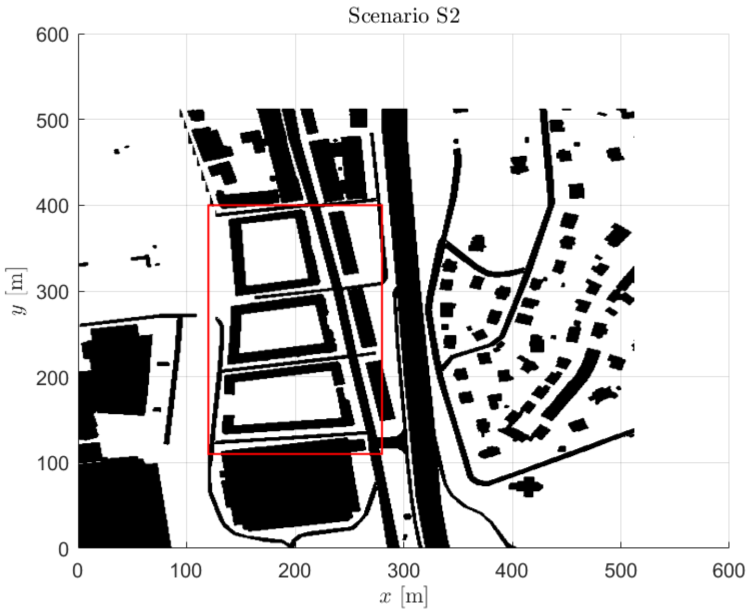

Figure 3.5: *Scenario S2, the red rectangle represents the area of interest.*

In S3, the houses to the west of Fabriksgatan are the same as in S2 and the houses at the other side of the street are wider than in S2 and now forms a wall against the highway (they are also shorter than in S2, between 10 m and 20 m). One of the houses have a courtyard. The scenario also has a wider street canyon. The scenario is shown in figure 3.6.

No vegetation or soil will be considered in the simple model, but a leaf area density is specified in the outskirts of the model. Emission and background data are example values, and the results will thus not reflect the actual values, but instead indicate which scenario that has the highest, respectively the lowest pollution levels.

3.5 Description of advanced model

In the advanced model, nesting will be used. In nesting, there is a parent model and child models. The parent model has a coarser grid over a larger area and the child models have finer grid over a smaller area of interest (PALM group, 2021d). This way, is it possible to both have a large domain and a fine grid in the area of interest, without being as computational expensive as a large domain with a fine grid. In this project, multi-scale self nesting with one child domain will be used, meaning that the parent and child domain run in parallel.

The parent domain will be 2048 m in the x-direction (west-east) and 1024 m in the y-direction (south-north) and the grid spacing will be 4 m in both directions,

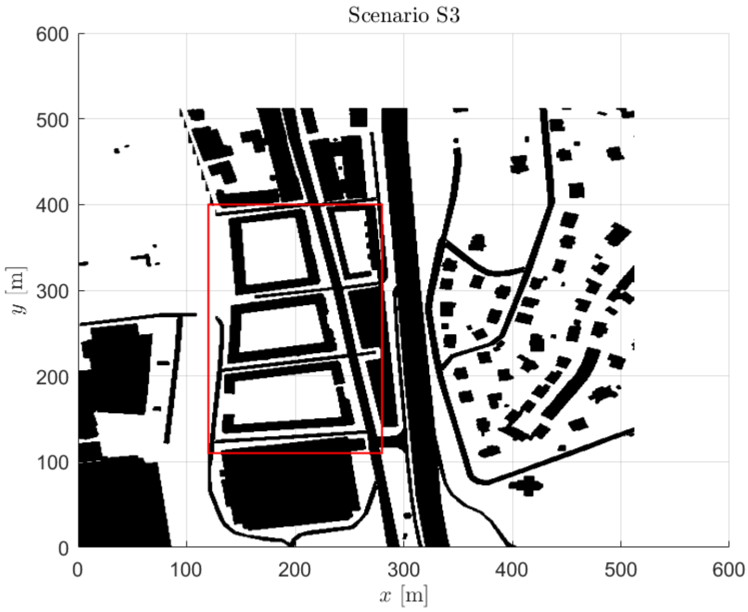

Figure 3.6: *Scenario S3, the red rectangle represents the area of interest.*

meaning that there will be 512 grid points in the x-direction and 256 grid points in the y-direction. In the z-direction, there will be 150 grid points. The grid spacing will be 4 m at the beginning, but after 228 m, the grid spacing will be stretched with 4% for every step, resulting in a high vertical domain (4273 m).

The child domain will be 512 m in the x-direction, 512 m in the y-direction and 128 m in the z-direction. The grid spacing will be 1 m in all directions and there will be no grid stretching in the z-direction, implying that there will be 512 grid points in the x-direction, 512 grid points in the y-direction and 128 grid points in the z-direction. The location of the child model with respect to the parent model is that the lower left corner of the child model is 932 m to the right of and 300 m above the lower left corner of the parent model. Both models starts at $z = 0$ m.

The two domains are shown in figure 3.7, where the black rectangle represents the parent domain and the red rectangle represents the child domain. Green areas correspond to different kinds of vegetation (evergreen and deciduous trees and grass). Yellow areas correspond to water and orange areas correspond to bare soil. Lighter blue areas correspond to buildings and darker blue areas correspond to streets and pavements.

Three extra scenarios will also be investigated in the advanced model, scenario *S4*, *S5* and *S6*. S4 is roughly the same as in scenario S0 but with a larger distance between the houses on both sides of Fabriksgatan, to make room for a row of trees and a bike- and walkway. The main houses in the area of interest are mainly between 10 m and 15 m high. The scenario is shown in figure 3.8. The red polygon represents the area of interest in the advanced model. Note that this area is smaller than in the simple model and centered along Fabriksgatan. This will be the focus area for all scenarios in the advanced model.

S5 is almost as S2 (meaning that the houses in the study area are between 20 m and 25 m high), but with a narrower street (the same width as in S0), meaning that

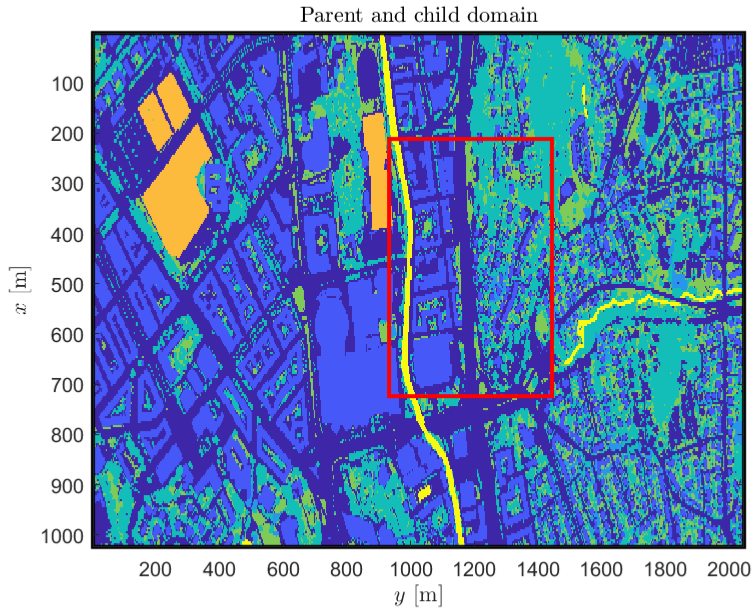

Figure 3.7: *The black rectangle represents the parent domain and the red rectangle represents the child domain.*

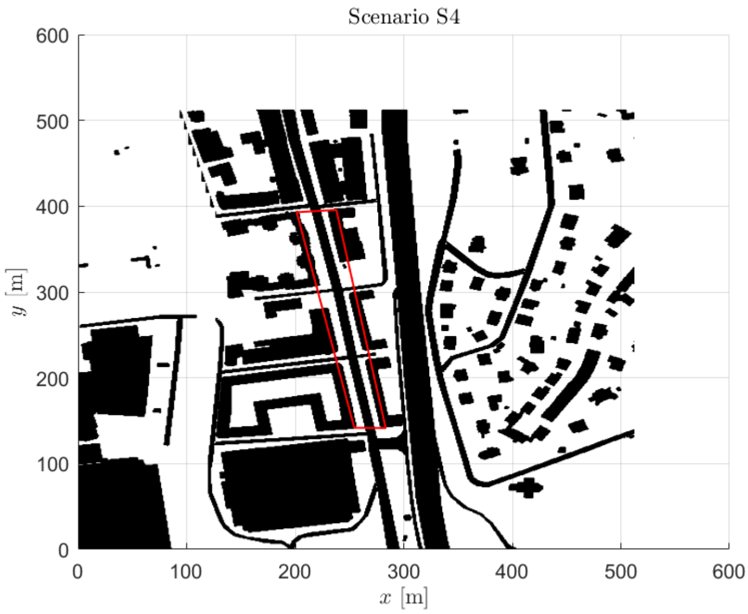

Figure 3.8: *Scenario S4, the red polygon represents the area of interest.*

there is no room for a row of trees. The scenario is shown in figure 3.9. S6 is a mix-up of S1 and S3. It has almost the same point houses to the west of Fabriksgatan as S1 (which are between 20 m and 30 m, but two extra houses) and the same houses to the east of Fabriksgatan as S3 (which are between 10 m and 20 m) and a wide street-canyon, see figure 3.10.

As already mentioned, the advanced model includes additional models in PALM, such as the land surface model, the radiation model, the urban surface model and

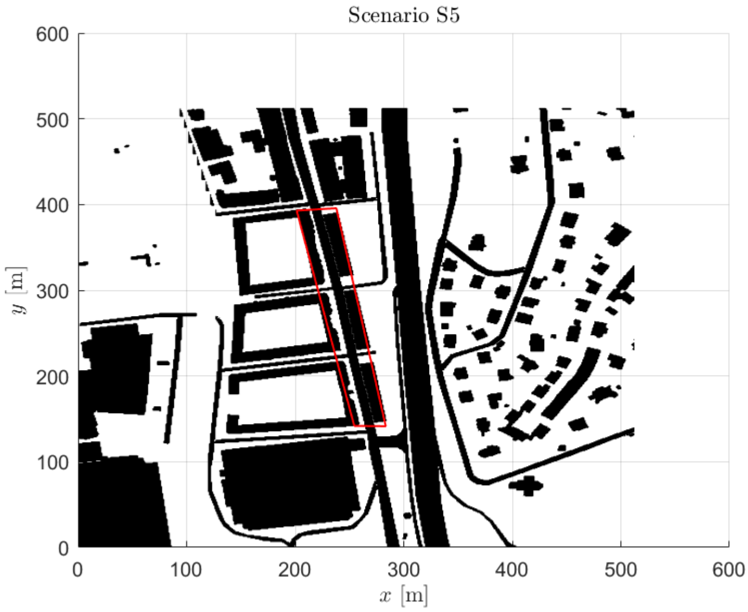

Figure 3.9: *Scenario S5, the red polygon represents the area of interest.*

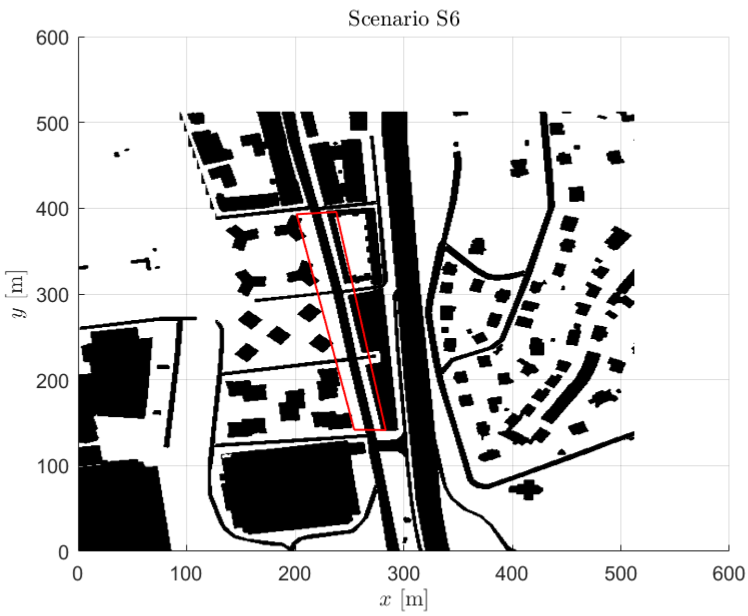

Figure 3.10: *Scenario S6, the red polygon represents the area of interest.*

a more detailed setup of the plant canopy model and the chemistry model. Thus, more parameters are needed to be specified, in order to run the model properly. These parameters will be described in the following sections.

3.5.1 Building type

The buildings will now be classified into different types for the child model. In the simple model were all buildings the default value, corresponding to a residential building from before 1950. In the advanced setup of scenario S0, the buildings are divided into three types, see figure 3.11. Green corresponds to residential building from before 1950, red corresponds to residential building from between 1951 and 2000 and blue corresponds to office building from between 1951 and 2000. The building type will affect the albedo of the building, but this is not implemented in the current PALM version (PALM group, 2021i). Thus, this division is only for future simulations.

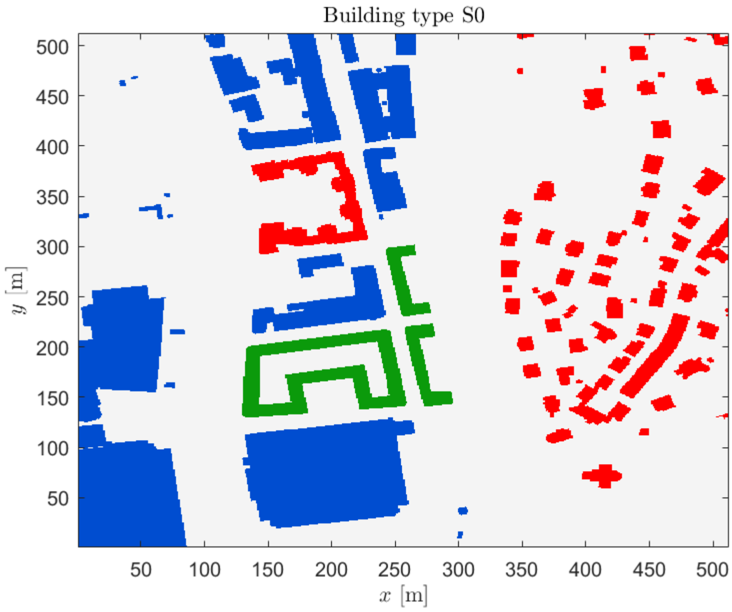

Figure 3.11: *The three building types in scenario S0. Green corresponds to residential building from before 1950, red corresponds to residential building from between 1951 and 2000 and blue corresponds to office building from between 1951 and 2000.*

In the advanced setup of scenario S1, S2, S3, S5 and S6, the three blocks that changes to the west of Fabriksgatan will be classified as residential buildings, constructed 2001 or later and the three blocks that changes to the right of Fabriksgatan will be classified as office buildings from 2001 and later. All are classified as of 2001 and after since they are supposed to be new houses. The office buildings are situated closer to the highway than the residential buildings since that is usually the case. In scenario S4, the building type will be the same as in scenario S0. Figure 3.12 shows the classification for scenario S1, but as previously mentioned, the classification will be the same for S2, S3, S5 and S6 as well.

In the parent domain all buildings will be considered as residential from 1951 to 2000.

3.5.2 Soil type, depth, temperature and moisture

In the area of interest, the soil consist mainly of post glacial and glacial sediments (Sveriges geologiska undersökning, 2021), which corresponds to fine soil in PALM. The difference between the two sediments is that the glacial sediments are sediments

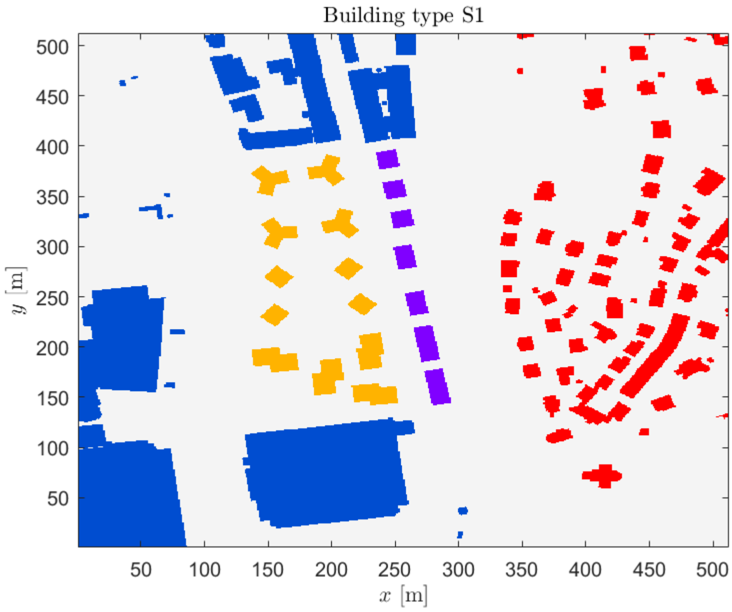

Figure 3.12: *The four building types in scenario S1. Orange corresponds to residential buildings constructed 2001 or later, purple corresponds to office buildings from 2001 and after, red corresponds to residential buildings built between 1951 and 2000 and blue corresponds to office buildings constructed between 1951 and 2000.*

originating from when the ice sheet from the latest ice age melted and the post glacial sediments originates from after the melting (Sveriges geologiska undersökning, 2020).

The soil will consist of eight layers , where the depth of each layer is 1 cm, 1 cm, 3 cm, 5 cm, 10 cm, 20 cm, 40 cm and 120 cm, meaning that the total depth is 200 cm.

In June 2019, the soil temperature was 290.5 K for the first 10 cm in the region (IRI/LDEO Climate Data Library, 2021b) and 283.1 K for 10 cm down to 200 cm (IRI/LDEO Climate Data Library, 2021d). In order to prevent inversion, a higher soil temperature must be set. With a lower soil temperature, signs of inversion were seen which is not realistic for a sunny summer day. For 0 cm to 1 cm, the temperature is set to 305 K, for 1 cm to 2 cm 304 K, for 2 cm to 5 cm 302 K, for 5 cm to 10 cm 301 K, for 10 cm to 20 cm 300 K, for 20 cm to 40 cm 297 K, for 40 cm to 80 cm 292 K and for 80 cm to 2 m 285 K. The deep soil temperature is set to the lowest value, 285 K. The soil moisture was for the same period 25.4% for the first 10 cm (IRI/LDEO Climate Data Library, 2021a) and 22.8% 10 cm down to 200 cm (IRI/LDEO Climate Data Library, 2021c), which will be used for the simulations.

The water content in the soil and atmosphere will be conserved during the simulations.

3.5.3 Vegetation type and root fraction

The vegetation in the area consists of evergreen and deciduous trees and grassland (S. Johansson, 2018). The trees are assumed to be broadleaved and the grassland is assumed to be short, to be able to classify it in PALM. The root fraction (the height distribution of the roots within the soil levels) is the average of the root fraction for deciduous broadleaved trees and short grassland, according to PALM group (2021c). The values for the root fraction will not be perfectly aligned with the soil depth, the values for down to 7 cm will be used down to 10 cm, the values for 7 cm to 28 cm will be used for 10 cm to 40 cm, the values for 28 cm to 1 m will be used for 40 cm to 80 cm and the values for 1 m to 2.89 m will be used from 80 cm to 2 m.

3.5.4 Vegetation scenarios

3.5.4.1 Inner domain

In the S0 scenario, representing the area today, there will be some vegetation, specified by the leaf area density, in the outskirts of the model. This vegetation is considered to be common lime, with a leaf area density of $0.67\,\mathrm{m}^2/\mathrm{m}^3$ (Klingberg et al., 2017). The S5 scenario will also have this limited amount of vegetation. The other building scenarios will have three vegetation scenarios each. One base scenario, with vegetation between the houses and no vegetation along Fabriksgatan, see figure 3.13. This vegetation will have a leaf area density of $0.67\,\mathrm{m}^2/\mathrm{m}^3$. One scenario with (in addition to the base vegetation) a sparse row of trees along Fabriksgatan (see figure 3.14) and one scenario with the base vegetation and a dense row of trees along Fabriksgatan (see figure 3.15). In all three figures, blue will correspond to buildings and green to vegetation. The row of trees consists of English oaks. For English oak, the leaf area density is $1.56\,\mathrm{m}^2/\mathrm{m}^3$ (Klingberg et al., 2017). The canopy of the row of trees is located between $z = 5.5\,\mathrm{m}$ and $z = 16.5\,\mathrm{m}$.

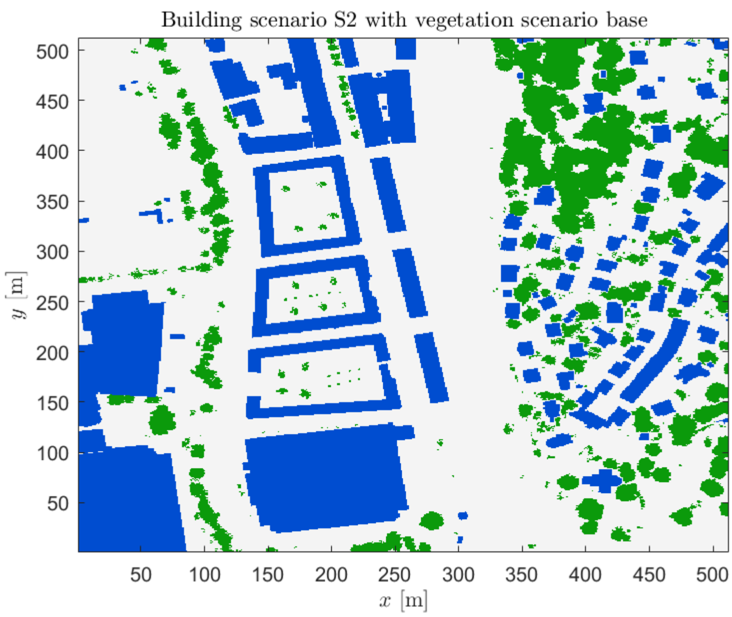

Figure 3.13: *The vegetation base scenario for scenario S2, where there is vegetation between the houses but no vegetation along Fabriksgatan. Blue corresponds to buildings and green to vegetation. All vegetation have a leaf area density of* $0.67\,\mathrm{m}^2/\mathrm{m}^3$.

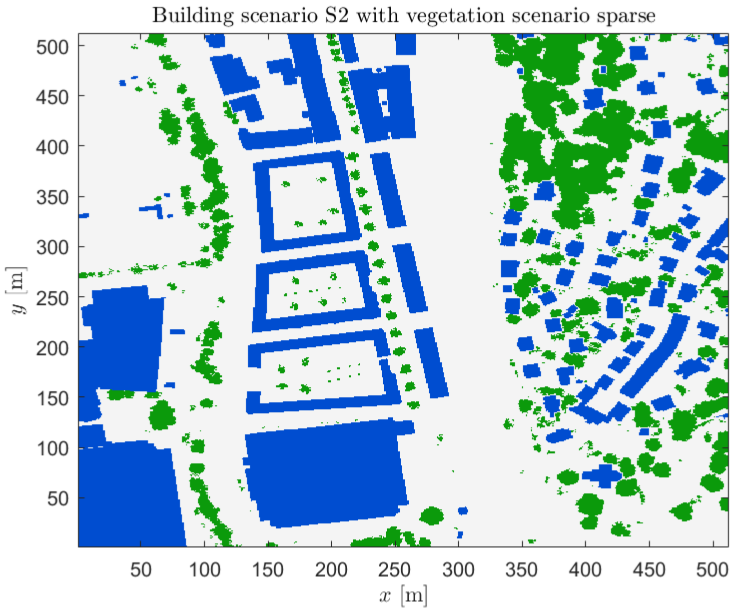

Figure 3.14: *The vegetation scenario for scenario S2 with a sparse row of trees, where there is vegetation between the houses and a sparse row of trees along Fabriksgatan. Blue corresponds to buildings and green to vegetation. All vegetation except the row of trees is assumed to be common lime, with a leaf area density of* $0.67\,\mathrm{m^2/m^3}$. *The row of trees consists of English oaks, with a leaf area density of* $1.56\,\mathrm{m^2/m^3}$.

Green walls will be investigated for building scenario S3, where buildings in the focus area will have a green wall of ivy on the side facing the street (see figure 3.16 where these buildings are colored green). Ivy is considered suitable for green walls, according to Abhijith et al. (2017). Ivy has a leaf area index of 3.5 to $4.0\,\mathrm{m^2/m^2}$ (Pérez et al., 2017) and $3.5\,\mathrm{m^2/m^2}$ will be used here. To go from leaf area index to leaf area density, the leaf area density is assumed to be constant through the canopy (as in Santiago, Martilli, and Martin (2017)). The green walls have a thickness of $1.0\,\mathrm{m}$, thus the leaf area density is $3.5\,\mathrm{m^2/m^2}/1\,\mathrm{m} = 3.5\,\mathrm{m^2/m^3}$. The rather large thickness is due to that this is the smallest resolution in PALM.

A CDSM file is used to get the vegetation height and then the leaf area density is set at each whole meter to the prescribed value up to that height. The first 5 m needs to be vegetation free in a city, for traffic to pass. Thus, the leaf area density is set to zero up to 5 m, except for the green walls. Thus, the leaf area density is constant and do not vary with height in the inner domain.

3.5.4.2 Outer domain

For leaf area density in the outer domain, data from Klingberg et al., 2017 is used. As in the inner domain, the leaf area density is set to zero up to 5 m.

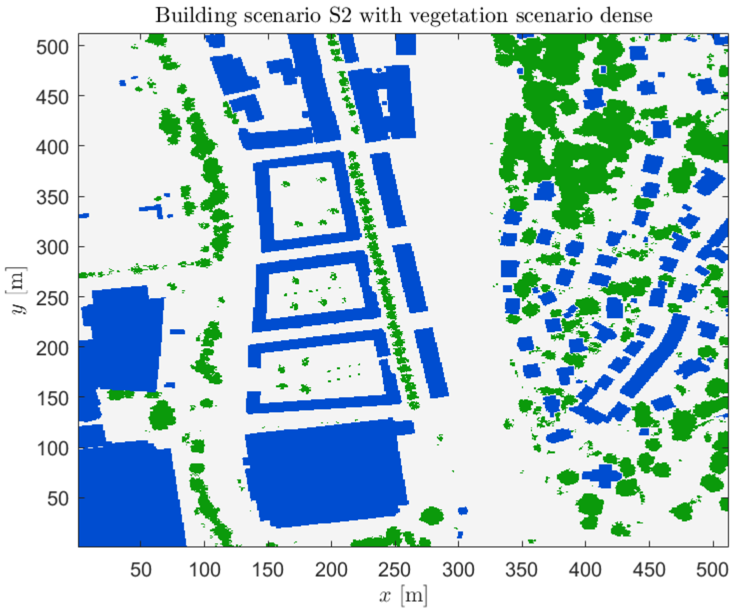

Figure 3.15: *The vegetation scenario for scenario S2 with a dense row of trees, where there is vegetation between the houses and a dense row of trees along Fabriksgatan. Blue corresponds to buildings and green to vegetation. All vegetation except the row of trees is common lime, with a leaf area density of* $0.67\,\mathrm{m}^2/\mathrm{m}^3$*. The row of trees consists of English oaks, with a leaf area density of* $1.56\,\mathrm{m}^2/\mathrm{m}^3$*.*

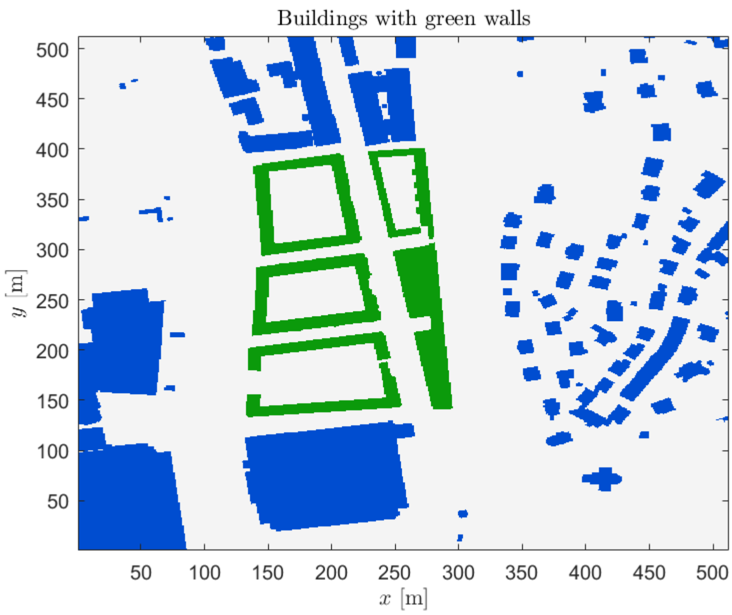

Figure 3.16: *The green buildings have a* $1\,\mathrm{m}$ *thick green wall made of ivy at the side facing Fabriksgatan.*

3.5.5 Water type

The water type lake will be used for the stream Mölndalsån, since that water type is the only water type implemented by PALM so far. The water temperature will be 305 K, constant during the simulations. This temperature is a bit higher than the true value, to prevent inversion.

3.5.6 Street and pavement type

The motorway is seen as the main road and all the other roads as side roads. The pavement type is assumed to be a mixture of asphalt and concrete.

3.5.7 Albedo

Surface albedo will be automatically set by PALM, depending on the vegetation, pavement, water and building type. For the chosen pavement type the albedo will be 0.17, for the chosen water type 0.06, and for the bare soil 0.08. For the chosen vegetation types the albedo will be 0.17 for the broadleaved deciduous trees, 0.14 for the broadleaved evergreen trees, and 0.25 for the short grass. For the buildings, the albedo will be 0.17 (PALM group, 2021f).

3.6 Background and emission data

Data on the background concentrations are obtained from SMHI, n.d.(a) where the measurement stations Göteborg Femman and Göteborg Haga are used both for the inner and outer domain. There is actually a measure station located in the inner domain but since that one is located almost at the motorway, those values are considered as too high to be representable for the full inner domain. Göteborg Haga is located 3 m above the surface and measures NOx, NO_2, $PM_{2.5}$ and PM_{10} and Göteborg Femman (located 31 m above the surface) measures the same and O_3. The values for NO are obtained by subtracting the values for NO_2 from NOx. An average is calculated by taking an average of the concentrations sunny days between 9.00 am and 11.00 am, starting 1 June 2019 and ending 30 June 2019 (to get the average background concentration at 10.00 am). To find sunny days, weather data for June 2019 from SMHI (n.d.[b]) is studied. First, days with precipitation between 9.00 am and 11.00 am were discarded (only four days) and then days where the solar radiation was below 400 W/m^2 were discarded (five days). Left were 21 days. Measurement values smaller than zero are considered as errors and are discarded.

To find height distributions for the concentrations, data from Inness et al., 2019 was used. In their data, values for concentration of NO, NO_2, and O_3 are given at the following heights: 10.00 m, 34.97 m, 71.89 m and 124.48 m (ECMWF, n.d.). The method to obtain height distributions was to assume that the surface value is the same as the value at 10.00 m, using the value from Göteborg Haga for NO and NO_2 at those heights (since Göteborg Haga is located at 3 m, the value is assumed to be the same at 0 m as well). Then ratios between the concentration at 71.89 m and 124.48 m compared to the value at 34.97 m were calculated (for O_3, the ratio between 10.00 m and 34.97 m was calculated as well). These ratios were then multiplied by each value obtained from (SMHI, n.d.[a]) for Göteborg Femman (located at around 30 m). This way, values at 34.97 m, 71.89 m and 124.48 m were obtained. These were then combined with the values for 0 m and 10 m (except for O_3, where the method for higher heights where used for 10 m as well and then assumed to be valid at 0 m too) to obtain height distributions for NO, NO_2, and O_3 at 0 m, 10 m, 35 m, 72 m and 124 m (the heights are rounded to the nearest integer). To obtain height distributions for PM_{10} and $PM_{2.5}$, data from Kurppa, Roldin, et al., 2020 was used. They measured lung-deposited surface area of aerosol particles at 0 m, 4 m, 8 m, 12 m, 16 m, 20 m, 24 m, 28 m, 32 m, 36 m, 40 m, 44 m and 48 m. The ratio between the concentration at each level and the concentration at the surface level were calculated and multiplied by the surface values for PM_{10} and $PM_{2.5}$ (obtained from (SMHI, n.d.[a]) at Göteborg Haga and assuming that they are valid at 0 m even if the measure station is located at 3 m). Thus, the ratios were assumed to be the same for both PM_{10} and $PM_{2.5}$ (but with a different scaling factor since the surface values differ).

Emission data from the motorway and from the street Fabriksgatan are obtained from a file that was created using data from HBEFA (n.d.), Göteborg Stad (n.d.) and SCB (n.d.). The file contains data for NO, NO_2 and PM_{10} in exhausts (there are no emissions of O_3) in g/day. Thus, $PM_{2.5}$ were not specified, but the amount of PM_{10} in exhausts were. Since exhaust particles are fine, they are assumed to all be $PM_{2.5}$. To get the rest of PM_{10}, data from simulated resuspension with NORTRIP (described in Denby et al. (2013)) were obtained. The data from the motorway is going to be used at the main street (the motorway) and the data from Fabriksgatan is going to be used at the side streets (which are the rest of the streets). The values needs to be in µmol/(m^2·day) for gases and kg/(m^2·day) for particulate matter to be compatible with the chemistry module in PALM. The values are thus converted, using the conversion factors in Appendix A. An average of the emissions at the motorway and at Fabriksgatan is calculated since PALM needs one emission value. Two fractions (for each chemical species) are then calculated, to obtain how much of the average that should be on the main street (that factor is larger than one) and how much of the average that should be on the side streets (that factor is smaller than one). PALM then takes the emission value and multiplies that value with the respective fraction. For the emission scenario with 10% less traffic, the emission data is multiplied by 0.9, to decrease it with 10%. For the emission scenario with 10% more traffic but with half of the vehicles as electric vehicles, the emissions of $PM_{2.5}$ and PM_{10} from electric vehicles are assumed to be the same as for the vehicles today. Those values are thus multiplied by 1.10 (to increase it with 10%). There will be no emissions of NO and NO_2 from electric vehicles, meaning that those values are multiplied by $0.5 \cdot 1.10 = 0.55$ (to cover a traffic increase of 10% and that 50% of the vehicles are electric vehicles). An emission scenario with the same traffic volume as today but 50% electric vehicles is also considered, and in that scenario, emissions of NO and NO_2 are multiplied by 0.5 and emissions of PM_{10} and $PM_{2.5}$ are multiplied by 1.0. The background data is assumed to be the same in all scenarios.

3.7 Relative humidity

In order to check that there is no cloud formation in the model, the relative humidity (the ratio between the humidity and the maximal humidity at that temperature) is studied. If this is well below 100%, cloud formation is avoided (National Weather

Service, n.d.).

3.8 Origin values

Origin values for x and y for the lower left corner of the smaller domain are 149402 and 6397637 in SWEREF 99 12 00. The latitude is 57.6979 degrees north and the longitude is 11.9986 degrees east. For the outer domain is $x = 148470$ and $y = 6397337$. The latitude is 57.6952 degrees north and the longitude is 11.9829 degrees east for the outer domain.

3.9 Water vapor mixing ratio and surface temperature

For the surface water vapor mixing ratio, a value of 0.7% will be used (the mean surface value for this parameter in the region in June 2019 (Hersbach et al., 2018)). This ratio is the ratio between the mass of surface water vapor and the mass of the dry air. The surface temperature is set to 303.0 K, a bit higher than the usual surface temperature to prevent inversion.

3.10 Boundary conditions

The bottom boundary condition for the water vapor mixing ratio will be a Dirichlet condition for both domains, meaning that it will be the prescribed surface value during the simulations. For the top boundary, a Neumann condition is applied for the outer domain (the value is calculated from the prescribed surface value, described in PALM group (2021j)) and a nested condition in the inner domain. A nested condition means that boundary conditions are obtained from the corresponding grid points in the outer domain (PALM group, 2021d).

For the bottom boundary condition for the potential surface temperature is a Dirichlet condition used for both domains, meaning that the potential surface temperature will be the prescribed surface value during the simulations. For the top, the boundary condition will be 'initial gradient' for the outer domain (the potential temperature is calculated from the prescribed surface value, described in PALM group (2021j) and for the inner domain, a nested condition will be used).

Along the x-axis, a cyclic boundary condition will be applied for all quantities (except the chemical species concentration) for the outer domain, meaning that what exits the right boundary will enter the left boundary, and vice versa. For the inner domain, a nested condition will be used. The same applies for the y-axis, meaning that what exits the north boundary will enter the south boundary (and the other way around) in the outer domain, and a nested condition in the inner domain.

For the chemical species concentration, Neumann conditions will be applied at the bottom, for both domains (meaning that the concentration changes at the bottom during the simulation, because of emissions). There will be Neumann conditions for the top in both domains as well. The left, right, north, and south boundary will have Dirichlet boundary conditions for both domains, which means that the chemical species concentration for the inflow will be constant during the simulation (given by the initial profiles).

For the turbulent kinetic energy, a Neumann condition will be used at the bottom in both domains. This will also hold for the bottom boundary condition for the perturbation pressure. For the top boundary condition for the perturbation pressure, a Dirichlet condition will be used for the outer domain, meaning that the pressure becomes zero at the top (PALM group, 2021j) and a Neumann condition for the inner domain.

For the horizontal velocity components (u and v), a Dirichlet no-slip condition will be used for both domains at the bottom, meaning that $u = v = 0\,\mathrm{m/s}$ (PALM group, 2021j). For the top, a Dirichlet condition will be used for the outer domain, but without the no-slip condition and that u is equal to the x-component of the geostrophic wind and that v is equal to the y-component of the geostrophic wind (PALM group, 2021j), and a nested boundary condition for the inner domain.

3.11 Initial conditions

Constant profiles are set at the beginning of the run with the above-mentioned values for soil temperature (water temperature will be constant during the run), the water vapor mixing ratio and the pollution levels (by using the background data). Constant profiles will also be set for the wind, and this will vary among the runs between 1.0 m/s, 2.5 m/s and 5.0 m/s, both west and east.

3.12 Simulation time

First, a two-hour spin-up of soil and wall temperature will run. With this spin-up, the temperature is adjusted to atmospheric conditions before the actual simulation starts, making the calculation faster (PALM group, 2021j). After that, the simulations will run for two hours (between 10.00 and 12.00). Data will be collected as a mean value for the second hour, since the first hour is regarded as another spin-up.

Chapter 4

Results

The results will first be presented for the simple model, and then more thoroughly for the advanced model.

4.1 Simple model

For the simple model, mean concentrations of NO, NO_2, O_3 and PM_{10} are calculated within the area of interest (specified by the red rectangle in for example figure 3.3) for $z = 1.5\,\mathrm{m}$ and a west wind of $2.5\,\mathrm{m/s}$. The results are presented in table 4.1. For each pollutant, the scenario with the highest concentration is marked in red, the second highest in orange and then follows yellow and green. For O_3, two scenarios with the same value are marked in different colours and this is since with more decimals, S2 has higher concentrations of O_3 than S3. Pollution levels are generally highest in scenario S3, second highest in scenario S2, and S0 and S1 alternating between lowest and second lowest levels.

Table 4.1: *Mean concentrations of NO (in ppm), NO_2 (in ppm), O_3 (in ppm) and PM_{10} (in $\mu\mathrm{g/m^3}$) for $z = 1.5\,\mathrm{m}$ for the building scenario S0, S1, S2 and S3 and $2.5\,\mathrm{m/s}$ west wind in the simple model. Standard deviations are also included.*

	S0	S1	S2	S3
NO [ppm]	0.080(097)	0.081(135)	0.091(137)	0.117(209)
NO_2 [ppm]	0.054(034)	0.051(043)	0.056(045)	0.062(061)
O_3 [ppm]	0.033(011)	0.036(011)	0.034(013)	0.034(013)
PM_{10} [$\mu\mathrm{g/m^3}$]	43.023(23.435)	41.943(31.320)	44.897(32.157)	50.903(47.863)

4.2 Advanced model

First, all pollutants (NO, NO_2, O_3, PM_{10} and $PM_{2.5}$) will be studied for all building and vegetation scenarios for a west wind of $2.5\,\mathrm{m/s}$ and at $z = 1.5\,\mathrm{m}$. Then, the pollutants are restricted to PM_{10} (and in some cases NO_2) to keep the result section smaller. The results will be presented both as relative mean concentrations with standard deviations, compared to a base scenario and also as point concentrations.

The topography is taken into account in the input file, but not for the output file. This means that the output data matrix will not have values everywhere at the first layers (if the topography is higher than the layer, the value will be NaN). Thus, for every point in the xy-plane, the second level with with existing values is used to calculate the mean concentration (since the first level with value represents 0.5 m and the grid spacing is 1.0 m).

Five point concentrations are studied. For scenario S0 and S5, where there is a narrow street canyon with no room for trees, two points at the road and three points at the west side of the street canyon are studied. The points are visualised for S0 in figure 4.1, where yellow corresponds to buildings and turquoise to roads. Note, that for S5 the locations are the same. For scenario S1, S2, S3, S4 and S6, with a wider street canyon with room for trees, there is a walk- and bikeway to the west of the row of trees. Two points at this walk- and bikeway, two points at the road and one point under the trees (in the base scenarios without a row of trees, this is just at the same location) are studied. In figure 4.2, the location of the points are visualised for scenario S2 dense. The locations will be the same for all S1, S2, S3, S4 and S6 scenarios, both for the base, dense and sparse vegetation scenarios. Even here, yellow areas correspond to buildings and turquoise to roads. Green areas correspond to vegetation, both the row of trees and vegetation in the courtyards.

Different scenarios will be compared, and concentrations will be presented in tables. If two scenarios are compared, the one with the highest value is coloured in red and the lowest in green. If they have the same value, both are yellow. If three scenarios are compared, the highest is red, the scenario in the middle is yellow and the lowest is green. For four scenarios, the colours are red, orange, yellow and green and for five scenarios, blue is added for the lowest value. For six scenarios, the colours are red, orange, yellow, green, dark green and blue.

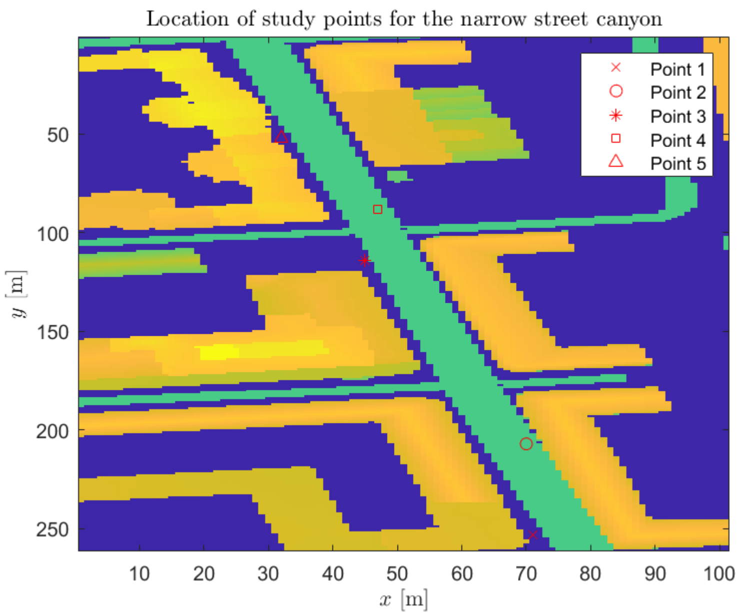

Figure 4.1: *Location of study points for the narrow street canyon. Point 1, 3 and 5 are located to the west of the road and point 2 and 4 are located on the road.*

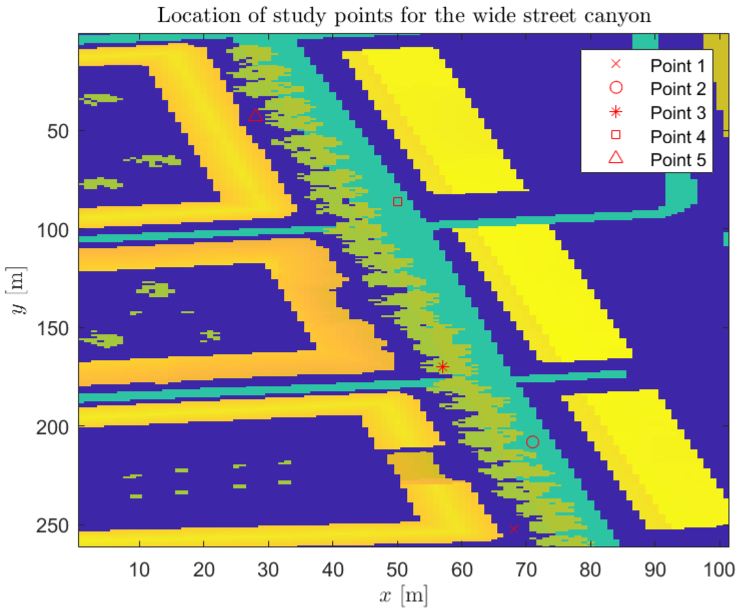

Figure 4.2: *Location of study points for the wide street canyon. Point 1, 3 and 5 are located to the west of the road and point 2 and 4 are located on the road.*

But first, the relative humidity will be studied.

4.2.1 Relative humidity

The relative humidity is investigated for ten scenarios, for both the inner and outer domain. The relative humidity is obtained as a horizontal average (for each point in the xy-plane) for height $z = 0\,\text{m}$, $z = 0.5\,\text{m}$, $z = 1.5\,\text{m}$,..., $z = 128.5\,\text{m}$ and time $t = 1000\,\text{s}$, $t = 2000\,\text{s}$,..., $t = 7000\,\text{s}$. The maximum values are then studied for the ten scenarios and presented in table 4.2.

Table 4.2: *Maximum value of the relative humidity (in %) for ten different building, vegetation and wind configurations, for both inner and outer domain.*

	Inner domain	Outer domain
S0 west 2.5 m/s	25.483	36.380
S1 base west 2.5 m/s	25.410	36.636
S2 base west 5 m/s	25.451	36.289
S2 dense west 1 m/s	25.522	36.694
S2 sparse east 2.5 m/s	25.619	36.527
S3 sparse west 2.5 m/s	25.536	36.497
S3 dense east 2.5 m/s	25.517	36.650
S4 base east 2.5 m/s	25.505	36.540
S5 west 2.5 m/s	25.557	36.497
S6 base west 2.5 m/s	25.513	36.637

The values for the relative humidity are all below 40%.

4.2.2 Pollution levels for different building and vegetation scenarios

All building and vegetation scenarios are studied for a west wind of 2.5 m/s. The concentration in the focus area at $z = 1.5$ m is highest for all pollutants except O_3 in scenario S5, and then S0. In a shared third place are S2 and S3, followed by S4 and then S6 and S1. Concentrations are usually highest for vegetation scenario dense and lower for scenario base and sparse. The results are displayed in the following tables.

S4 base and S0 are similar, except a bit more background vegetation in S4 base than in S0 and that S4 base has a wider street than S0 (the same street width as in S1, S2, S3 and S6). Thus, S4 base is more suitable for comparisons against the other scenarios than S0 is.

Table 4.3 shows the relative concentration of NO for $z = 1.5$ m for 2.5 m/s westerly wind for varying building and vegetation scenarios, compared to the S4 base scenario.

Table 4.3: *Relative concentration of NO for* $z = 1.5$ m *with* 2.5 m/s *west wind and with S4 base as base scenario for different building and vegetation scenarios.*

	S0	S1	S2	S3	S4	S5	S6
Base	1.647(509)	0.857(337)	1.073(253)	1.046(308)	1.000(262)	1.974(628)	0.930(385)
Dense	-	1.000(374)	1.236(293)	1.214(340)	1.183(352)	-	0.976(384)
Sparse	-	0.861(374)	1.076(345)	1.123(308)	1.051(342)	-	0.918(408)

Table 4.4 shows the relative concentration of NO_2 for $z = 1.5$ m for 2.5 m/s westerly wind for varying building and vegetation scenarios, compared to the S4 base scenario.

Table 4.4: *Relative concentration of* NO_2 *for* $z = 1.5$ m *with* 2.5 m/s *west wind and with S4 base as base scenario for different building and vegetation scenarios.*

	S0	S1	S2	S3	S4	S5	S6
Base	1.419(275)	0.883(156)	1.064(126)	1.038(139)	1.000(116)	1.610(304)	0.979(208)
Dense	-	1.016(196)	1.196(136)	1.187(169)	1.161(186)	-	1.016(203)
Sparse	-	0.879(194)	1.058(184)	1.121(140)	1.028(172)	-	0.921(205)

Table 4.5 shows the relative concentration of O_3 for $z = 1.5$ m for 2.5 m/s westerly wind for varying building and vegetation scenarios, compared to the S4 base scenario.

Table 4.5: *Relative concentration of* O_3 *for* $z = 1.5$ m *with* 2.5 m/s *west wind and with S4 base as base scenario for different building and vegetation scenarios.*

	S0	S1	S2	S3	S4	S5	S6
Base	0.931(045)	1.022(023)	0.989(022)	0.992(021)	1.000(019)	0.902(044)	1.001(033)
Dense	-	0.996(030)	0.964(023)	0.964(028)	0.970(032)	-	0.995(032)
Sparse	-	1.022(030)	0.990(031)	0.976(021)	0.996(029)	-	1.014(031)

Table 4.6 shows the relative concentration of PM_{10} for $z = 1.5\,\mathrm{m}$ for $2.5\,\mathrm{m/s}$ westerly wind for varying building and vegetation scenarios, compared to the S4 base scenario.

Table 4.6: *Relative concentration of PM10 for $z = 1.5\,\mathrm{m}$ with $2.5\,\mathrm{m/s}$ west wind and with S4 base as base scenario for different building and vegetation scenarios.*

	S0	S1	S2	S3	S4	S5	S6
Base	1.268(214)	0.935(132)	1.030(096)	1.032(121)	1.000(101)	1.411(252)	0.973(154)
Dense	-	0.982(144)	1.098(111)	1.101(135)	1.073(138)	-	0.986(152)
Sparse	-	0.933(146)	1.034(136)	1.063(120)	1.018(135)	-	0.962(162)

Table 4.7 shows the relative concentration of $PM_{2.5}$ for $z = 1.5\,\mathrm{m}$ for $2.5\,\mathrm{m/s}$ westerly wind for varying building and vegetation scenarios, compared to the S4 base scenario.

Table 4.7: *Relative concentration of $PM_{2.5}$ for $z = 1.5\,\mathrm{m}$ with $2.5\,\mathrm{m/s}$ west wind and with S4 base as base scenario for different building and vegetation scenarios.*

	S0	S1	S2	S3	S4	S5	S6
Base	1.064(044)	0.985(028)	1.009(022)	1.003(025)	1.000(021)	1.093(053)	0.995(034)
Dense	-	1.004(034)	1.027(024)	1.022(028)	1.022(030)	-	1.001(034)
Sparse	-	0.985(033)	1.008(030)	1.014(025)	1.005(028)	-	0.989(035)

4.2.3 Pollution levels for different building scenarios

Five point concentrations of PM_{10} are calculated for all building and vegetation scenarios. The concentrations vary a lot from point to point, which is seen in the following tables.

Table 4.8 shows five point concentrations of PM10 (in $\mu g/m^3$) for $z = 1.5\,\mathrm{m}$ with the vegetation base scenario and $2.5\,\mathrm{m/s}$ west wind, for the S1, S2, S3 and S4 building scenario.

Table 4.8: *Five point concentrations of PM_{10} (in $\mu g/m^3$) for $z = 1.5\,\mathrm{m}$ with the vegetation base scenario and $2.5\,\mathrm{m/s}$ west wind, for different building scenarios.*

	S1 base	S2 base	S3 base	S4 base	S6 base
Point 1	8.900	10.322	8.956	10.453	8.839
Point 2	10.672	10.316	10.065	9.298	10.690
Point 3	9.395	10.717	9.586	9.835	9.083
Point 4	9.698	10.085	10.748	10.207	11.171
Point 5	7.215	9.458	9.101	8.710	6.932

Scenario S0 and S5 has no base, dense and sparse vegetation scenario, just one scenario with a little vegetation in the outskirts (since there is no room for the row of trees). Thus, they are compared separately in table 4.9.

Table 4.9: *Five point concentrations of PM_{10} (in µg/m^3) for $z = 1.5$ m with 2.5 m/s west wind, for building scenario S0 and S5.*

	S0	S5
Point 1	12.368	11.292
Point 2	13.588	12.335
Point 3	9.671	10.259
Point 4	10.073	11.457
Point 5	14.994	14.543

Table 4.10 shows five point concentrations of PM_{10} (in µg/m^3) for $z = 1.5$ m with the vegetation sparse scenario and 2.5 m/s west wind, for S1, S2, S3 and S4 building scenario and S4 base as a base scenario for comparison.

Table 4.10: *Five point concentrations of PM_{10} (in µg/m^3) for $z = 1.5$ m with the vegetation sparse scenario and 2.5 m/s west wind, for different building scenarios.*

	S4 base	S1 sparse	S2 sparse	S3 sparse	S4 sparse	S6 sparse
Point 1	10.453	9.399	10.569	9.945	11.240	8.656
Point 2	9.298	9.821	9.871	9.956	9.452	10.275
Point 3	9.835	9.025	10.505	10.623	9.724	8.752
Point 4	10.207	10.754	10.020	10.046	9.830	11.184
Point 5	8.710	6.654	10.625	9.467	9.610	6.978

Table 4.11 shows five point concentrations of PM_{10} (in µg/m^3) for $z = 1.5$ m with the vegetation dense scenario and 2.5 m/s west wind, for S1, S2, S3 and S4 building scenario and S4 base as a base scenario for comparison.

Table 4.11: *Five point concentrations of PM_{10} (in µg/m^3) for $z = 1.5$ m with the vegetation dense scenario and 2.5 m/s west wind, for different building scenarios.*

	S4 base	S1 dense	S2 dense	S3 dense	S4 dense	S6 dense
Point 1	10.453	9.437	10.229	10.156	10.708	9.502
Point 2	9.298	10.842	10.599	9.780	10.688	11.422
Point 3	9.835	9.442	11.406	11.208	10.591	8.966
Point 4	10.207	10.054	9.734	10.719	9.592	11.531
Point 5	8.710	7.080	10.253	10.085	9.558	7.137

4.2.4 Pollution levels for different vegetation scenarios

Point concentrations are calculated for each building and vegetation scenario and presented in one table for each building scenario. For S1, S3 and S6 are a majority of the point concentrations highest in vegetation scenario dense. For scenario S2 and S4 are two points (point 2 and 3) highest for vegetation scenario dense and two points (point 1 and 5) highest for vegetation scenario sparse (and point 4 highest for vegetation scenario base).

Table 4.12 shows five point concentrations of PM_{10} (in µg/m^3) for $z = 1.5$ m with the building scenario S1 and 2.5 m/s west wind, for base vegetation, dense vegetation and sparse vegetation.

Table 4.12: *Five point concentrations of PM_{10} (in µg/m^3) for $z = 1.5$ m with the S1 building scenario and 2.5 m/s west wind, for different vegetation scenarios.*

	S1 base	S1 dense	S1 sparse
Point 1	8.900	9.437	9.399
Point 2	10.672	10.842	9.821
Point 3	9.395	9.442	9.025
Point 4	9.698	10.054	10.754
Point 5	7.215	7.080	6.654

Table 4.13 shows five point concentrations of PM_{10} (in µg/m^3) for $z = 1.5$ m with the building scenario S2 and 2.5 m/s west wind, for base vegetation, dense vegetation and sparse vegetation.

Table 4.13: *Five point concentrations of PM_{10} (in µg/m^3) for $z = 1.5$ m with the S2 building scenario and 2.5 m/s west wind, for different vegetation scenarios.*

	S2 base	S2 dense	S2 sparse
Point 1	10.322	10.229	10.569
Point 2	10.316	10.599	9.871
Point 3	10.717	11.406	10.505
Point 4	10.085	9.734	10.020
Point 5	9.458	10.253	10.625

Table 4.14 shows five point concentrations of PM_{10} (in µg/m^3) for $z = 1.5$ m with the building scenario S3 and 2.5 m/s west wind, for base vegetation, dense vegetation and sparse vegetation.

Table 4.14: *Five point concentrations of PM_{10} (in µg/m^3) for $z = 1.5$ m with the S3 building scenario and 2.5 m/s west wind, for different vegetation scenarios.*

	S3 base	S3 dense	S3 sparse
Point 1	8.956	10.156	9.945
Point 2	10.065	9.780	9.956
Point 3	9.586	11.208	10.623
Point 4	10.748	10.719	10.046
Point 5	9.101	10.085	9.467

Table 4.15 shows five point concentrations of PM_{10} (in µg/m^3) for $z = 1.5$ m with the building scenario S4 and 2.5 m/s west wind, for base vegetation, dense vegetation and sparse vegetation.

Table 4.16 shows five point concentrations of PM_{10} (in µg/m^3) for $z = 1.5$ m with the building scenario S6 and 2.5 m/s west wind, for base vegetation, dense vegetation and sparse vegetation.

Table 4.15: *Five point concentrations of PM_{10} (in µg/m^3) for $z = 1.5$ m with the S4 building scenario and 2.5 m/s west wind, for different vegetation scenarios.*

	S4 base	S4 dense	S4 sparse
Point 1	10.453	10.708	11.240
Point 2	9.230	10.688	9.452
Point 3	9.835	10.591	9.724
Point 4	10.207	9.592	9.830
Point 5	8.710	9.558	9.610

Table 4.16: *Five point concentrations of PM_{10} (in µg/m^3) for $z = 1.5$ m with the S6 building scenario and 2.5 m/s west wind, for different vegetation scenarios.*

	S6 base	S6 dense	S6 sparse
Point 1	8.839	9.502	8.656
Point 2	10.690	11.422	10.275
Point 3	9.083	8.966	8.752
Point 4	11.171	11.531	11.184
Point 5	6.932	7.137	6.978

4.2.5 Pollution levels for different wind configurations

Table 4.17 shows the relative concentration of PM_{10} for $z = 1.5$ m for S2 base and S2 dense, for various wind speeds and directions, compared to the S2 base scenario with 2.5 m/s west wind. Concentrations are generally higher for an eastern wind but the highest is obtained with a low western wind and a dense row of trees. The lowest concentration is obtained with a high western wind and no row of trees.

Table 4.17: *Relative concentration of PM_{10} for $z = 1.5$ m for S2 base and S2 dense for different wind speeds and directions.*

	S2 base	S2 dense
West 1.0 m/s	1.049(119)	1.129(144)
West 2.5 m/s	1.000(093)	1.066(108)
West 5.0 m/s	0.974(108)	0.987(139)
East 1.0 m/s	1.014(101)	1.082(127)
East 2.5 m/s	1.086(127)	1.107(143)
East 5.0 m/s	1.059(121)	1.114(143)

The wind configuration 2.5 m/s east is investigated for S3 base and S3 dense as well, and the results are presented in table 4.18. Here, S2 base is used as a reference scenario. The relative concentration is higher for both S2 scenarios, but highest for the scenario with a dense row of trees.

Table 4.19 shows five point concentrations of PM_{10} (in µg/m^3) for $z = 1.5$ m with the building scenario S2 and base vegetation scenario. Six different wind configurations are studied, 1 m/s west and east, 2.5 m/s west and east and 5 m/s west and east. Table 4.20 shows the same but for vegetation scenario dense. The point con-

Table 4.18: *Relative concentration of PM_{10} for $z = 1.5$ m for S2 base and S2 dense for different wind speeds and directions.*

	S2 base	S2 dense	S3 base	S3 dense
East 2.5 m/s	1.000(117)	1.020(132)	0.908(114)	0.958(100)

centrations vary from point to point but are generally lower for east winds and high for 1.0 m/s west wind for vegetation scenario dense. For both vegetation scenario base and dense, point 3 is highest for a moderate (2.5 m/s) and a high (5.0 m/s) western wind, while point 4 is highest for a low (1.0 m/s) western wind. Point 2 is highest for a moderate (2.5 m/s) and a high (5.0 m/s) eastern wind, while for a low 1.0 m/s) eastern wind, point 4 is highest for vegetation scenario base and point 3 highest for vegetation scenario dense.

Table 4.19: *Five point concentrations of PM_{10} (in $\mu g/m^3$) for $z = 1.5$ m with the S2 building scenario and base vegetation scenario for different wind configurations (+ indicates west wind and − indicates east wind).*

	+1.0 m/s	+2.5 m/s	+5.0 m/s	-1.0 m/s	-2.5 m/s	-5.0 m/s
Point 1	8.830	10.322	9.795	9.918	9.395	9.000
Point 2	9.881	10.316	9.209	9.545	11.439	11.583
Point 3	10.775	10.717	11.224	10.524	10.814	9.890
Point 4	10.858	10.085	9.087	11.149	11.123	10.598
Point 5	9.096	9.458	9.636	9.5246	8.951	8.991

Table 4.20: *Five point concentrations of PM_{10} (in $\mu g/m^3$) for $z = 1.5$ m with the S2 building scenario and dense vegetation scenario for different wind configurations (+ indicates west wind and − indicates east wind).*

	+1.0 m/s	+2.5 m/s	+5.0 m/s	-1.0 m/s	-2.5 m/s	-5.0 m/s
Point 1	10.596	10.229	9.921	9.109	9.920	8.686
Point 2	11.276	10.599	9.895	10.940	12.891	13.048
Point 3	10.557	11.406	10.915	11.518	11.025	10.607
Point 4	11.646	9.734	10.227	10.097	9.856	10.134
Point 5	11.436	10.253	10.562	10.294	10.033	9.733

4.2.6 Using buildings to block emissions

The ability of the buildings to block emissions are investigated for building scenario S3 and an east wind of 2.5 m/s. S3 has houses that almost forms a wall against the highway, see figure 3.6. By turning of emissions from all other roads than the highway, the concentration at Fabriksgatan is compared to that at Fabriksgatan when all emissions are on, which could be seen in the following tables. Concentrations (both point and relative) are lower when only emissions from the highway are applied and generally higher for S2 than for S3.

Table 4.21 shows the relative concentration of PM10 for $z = 1.5\,\mathrm{m}$ for S3 base and S3 dense, with emissions from all roads and emissions from only the highway for $2.5\,\mathrm{m/s}$ east wind, compared to S3 base with emissions from all roads and $2.5\,\mathrm{m/s}$ east wind. S2 base with emissions from all roads and emissions from only the highway is also added for comparison, since S2 has the same houses as S3 to the west of Fabriksgatan but not the same blocking houses to the right of Fabriksgatan.

Table 4.21: *Relative concentration of PM10 for $z = 1.5\,\mathrm{m}$ with $2.5\,\mathrm{m/s}$ east wind, S3 base, S3 dense and S2 base and with and without emissions from Fabriksgatan*

	S3 base	S3 dense	S2 base
Emissions from all roads	1.000(125)	1.056(110)	1.101(129)
Only emissions from highway	0.649(006)	0.650(013)	0.685(026)

Table 4.22 shows five point concentrations of PM10 (in $\mu\mathrm{g/m^3}$) for $z = 1.5\,\mathrm{m}$ with the building scenario S3 and $2.5\,\mathrm{m/s}$ east wind, for base and dense vegetation, with and without emissions from other roads than the highway.

Table 4.22: *Five point concentrations of PM_{10} (in $\mu\mathrm{g/m^3}$) for $z = 1.5\,\mathrm{m}$ with the S3 building scenario and $2.5\,\mathrm{m/s}$ east wind, for different vegetation and emission scenarios (* indicates only emissions from the highway).*

	S3 base*	S3 base	S3 dense*	S3 dense	S2 base*	S2 base
Point 1	6.216	8.206	6.408	8.895	6.823	9.395
Point 2	6.296	10.981	6.408	10.946	6.636	11.439
Point 3	6.261	9.541	6.217	10.146	6.628	10.814
Point 4	6.264	11.127	6.214	10.991	6.873	11.123
Point 5	6.311	7.710	6.177	9.402	6.384	8.951

4.2.7 Emission scenarios

Concentrations of NO_2 and PM_{10} are studied for different emission scenarios. Three for scenario S2 dense and two for scenario S3 dense, both with a westerly wind of $2.5\,\mathrm{m/s}$. Concentrations of NO_2 increases for emission scenarios with more vehicles using fossil fuels and decreases with emission scenarios with less vehicles using fossil fuels. Concentrations of PM_{10} increases for emission scenarios where the traffic increases, independent of whether the vehicles are electric or not, which could be seen in the following tables.

Table 4.23 shows the relative concentration of PM_{10} for $z = 1.5\,\mathrm{m}$ for S2 dense with $2.5\,\mathrm{m/s}$ west wind for today and two future emissions scenarios; one with 10% more traffic but 50% EV's and one with 10% less traffic but the same vehicle fleet, compared to today. Table 4.24 shows the relative concentration of NO_2 for the same configurations.

Table 4.25 shows the relative concentration of PM_{10} for two different emissions scenario for S3 dense; today and a scenario with the same traffic volume as today but with 50% EV's, compared to today. The wind is $2.5\,\mathrm{m/s}$ west. Table 4.26 shows the same but for NO_2.

Table 4.23: *Relative concentration of PM_{10} for $z = 1.5\,\mathrm{m}$ with S2 dense and $2.5\,\mathrm{m/s}$ west wind, for three emission scenarios.*

	PM_{10}
Today	1.000(101)
10% more traffic, 50% EV's	1.044(111)
10% less traffic	0.956(091)

Table 4.24: *Relative concentration of NO2 for $z = 1.5\,\mathrm{m}$ with S2 dense and $2.5\,\mathrm{m/s}$ west wind, for three emission scenarios.*

	NO_2
Today	1.000(114)
10% more traffic, 50% EV's	0.709(067)
10% less traffic	0.938(104)

Table 4.25: *Relative concentration of PM_{10} for $z = 1.5\,\mathrm{m}$ with S3 dense and $2.5\,\mathrm{m/s}$ west wind, for two emission scenarios.*

	PM_{10}
Today	1.000(122)
50% EV's	1.000(122)

Table 4.26: *Relative concentration of NO_2 for $z = 1.5\,\mathrm{m}$ with S3 dense and $2.5\,\mathrm{m/s}$ west wind, for two emission scenarios.*

	NO_2
Today	1.000(142)
50% EV's	0.672(076)

Table 4.27 shows five point concentrations of PM_{10} (in $\mu g/m^3$) for $z = 1.5\,\mathrm{m}$ with the building scenario S2 and vegetation scenario dense, for $2.5\,\mathrm{m/s}$ west wind and different emission scenarios. For NO_2 at point 4, the same value is marked as two different colours, that is because with more decimals, the cell marked in red has a higher concentration than the yellow cell.

Table 4.28 shows five point concentrations of PM_{10} (in $\mu g/m^3$) for $z = 1.5\,\mathrm{m}$ with the building scenario S3 and vegetation scenario dense, for $2.5\,\mathrm{m/s}$ west wind and different emission scenarios.

4.2.8 Green walls

Green walls are studied for scenario S3 base and $2.5\,\mathrm{m/s}$ west wind and are located as showed in figure 3.16. Table 4.29 shows the relative concentration of PM_{10} for S3 base, with and without green walls and $2.5\,\mathrm{m/s}$ west wind, with without green walls as the reference scenario. The relative concentration increases with greens wall.

Table 4.30 shows point concentrations of PM_{10} for S3 base, with and without green walls and $2.5\,\mathrm{m/s}$ west wind. A majority of the point concentrations are higher

Table 4.27: *Five point concentrations of PM_{10} (in µg/m^3) and NO_2 (in ppm) for $z = 1.5$ m with the S2 building scenario and 2.5 m/s west wind, for vegetation scenario dense and different emission scenarios.*

	Today	10% more traffic, 50% EV's	10% less traffic
Point 1 - PM_{10} [µg/m^3]	10.229	10.668	9.789
Point 2 - PM_{10} [µg/m^3]	10.599	11.065	10.132
Point 3 - PM_{10} [µg/m^3]	11.406	11.957	10.855
Point 4 - PM_{10} [µg/m^3]	9.734	10.113	9.356
Point 5 - PM_{10} [µg/m^3]	10.253	10.692	9.814
Point 1 - NO_2 [ppm]	0.013	0.009	0.012
Point 2 - NO_2 [ppm]	0.012	0.008	0.011
Point 3 - NO_2 [ppm]	0.013	0.009	0.012
Point 4 - NO_2 [ppm]	0.010	0.007	0.010
Point 5 - NO_2 [ppm]	0.012	0.008	0.011

Table 4.28: *Five point concentrations of PM_{10} (in µg/m^3) and NO_2 (in ppm) for $z = 1.5$ m with the S3 building scenario and 2.5 m/s west wind, for vegetation scenario dense and different emission scenarios.*

	Today	Same traffic volume, 50% EV's
Point 1 - PM_{10} [µg/m^3]	10.156	10.156
Point 2 - PM_{10} [µg/m^3]	9.780	9.780
Point 3 - PM_{10} [µg/m^3]	11.208	11.208
Point 4 - PM_{10} [µg/m^3]	10.719	10.719
Point 5 - PM_{10} [µg/m^3]	10.085	10.085
Point 1 - NO_2 [ppm]	0.013	0.008
Point 2 - NO_2 [ppm]	0.010	0.007
Point 3 - NO_2 [ppm]	0.013	0.009
Point 4 - NO_2 [ppm]	0.012	0.008
Point 5 - NO_2 [ppm]	0.012	0.008

Table 4.29: *Relative concentration of PM_{10} for $z = 1.5$ m with S3 base and 2.5 m/s west wind, with and without green walls.*

	PM_{10}
Without green wall	1.000(117)
With green wall	1.022(118)

with a green wall.

4.2.9 Ability of the row of trees to shield

The ability of the row of trees to act as a shield is also investigated. Two pair of points, at the same height ($z = 10.5$ m which is inside the canopy) and the same y-coordinate for both pairs, on both sides of the row of trees are investigated, for

Table 4.30: *Five point concentrations of PM_{10} (in µg/m^3) for $z = 1.5$ m with the S3 base scenario and 2.5 m/s west wind, for both without green walls and with green walls.*

	Without green wall	With green wall
Point 1	8.956	9.379
Point 2	10.065	10.813
Point 3	9.586	9.819
Point 4	10.748	10.727
Point 5	9.101	8.663

both western and eastern wind (of 2.5 m/s). The locations of the pair of points are presented in figure 4.3, where yellow areas correspond to buildings, turquoise areas to roads and green areas to vegetation. The chosen building scenario is S2 and the row of trees is dense. The results are presented in table 4.31. The cell with the higher concentration for each location and scenario is marked in red. The u-component of the velocity is also studied at those points, to see if the velocity changes when the wind passes through the row of trees. This is showed in table 4.32, where the arrows point to the left for eastern wind and to the right for western wind. The length of the arrow depends on the wind speed.

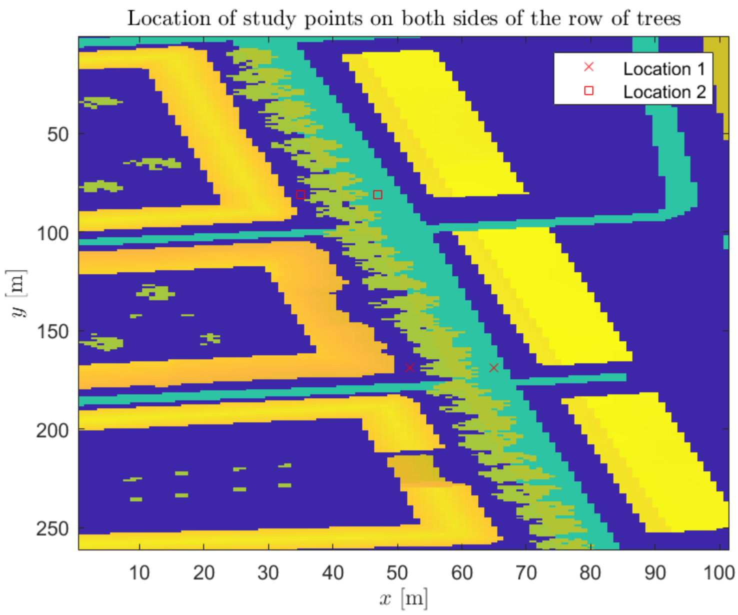

Figure 4.3: *Locations of the two pair of points that are used to investigate the ability of the row of trees to block pollution in the scenario S2 dense.*

In the first location, the concentration of PM_{10} has decreased by 12.2% on the leeward side for western wind, while it has increased by 6.1% for eastern wind. For the second location, the decrease is 8.5% for western wind and an increase of 0.6% for eastern wind.

By looking at table 4.32, the wind direction on both side of the row of trees could

Table 4.31: *Point concentrations of PM_{10} (in µg/m^3) for z = 10.5 m with the S2 building scenario and the dense vegetation scenario for 2.5 m/s west wind and 2.5 m/s east wind.*

	2.5 m/s west wind	2.5 m/s east wind
Location 1 - western side	9.633	9.170
Location 1 - eastern side	8.459	8.645
Location 2 - western side	8.672	7.857
Location 2 - eastern side	7.932	7.809

Table 4.32: *Point wind speeds (in m/s) in the x-direction for z = 10.5 m with the S2 building scenario and the dense vegetation scenario for 2.5 m/s west wind and 2.5 m/s east wind. Arrows pointing to the left indicate eastern wind and arrows pointing to the right indicate western wind. The length of the arrow depends on the wind speed.*

	2.5 m/s west wind	2.5 m/s east wind
Location 1 - western side	0.054 ⟶	0.016 →
Location 1 - eastern side	0.098 ⟶	⟵ -0.402
Location 2 - western side	0.020 →	0.013 →
Location 2 - eastern side	⟵ -0.059	⟵ -0.223

be studied. In location 1, the western wind is enhanced after the row of trees and the eastern wind is slowed down and turned into a western wind after the row of trees. In location 2, the western wind is slowed down and turned into an east wind after the row of trees. Also the east wind is reversed after the row of trees in the second location.

4.2.10 Detailed investigation of S2

Building scenario S2 is investigated in more detail. In figure 4.4, the differences between concentrations of PM_{10} in S2 dense and S2 base, S2 dense and S2 sparse and S2 sparse and S2 base are presented. The height is z = 1.5 m and the wind is 2.5 m/s west. The studied pollutant is PM_{10} (in µg/m^3). Yellow areas means that the concentration is higher in the first term and blue areas means that the concentration is higher in the second term.

The row of trees is located to the left in the street canyon (see figure 3.15 for the dense row and figure 3.14 for the sparse row). It could be seen in figure 4.4 that S2 dense has higher concentration of PM_{10} than S2 base for the row of trees. S2 sparse also has higher concentrations of PM_{10} than S2 base and also higher than S2 dense where the row of trees are. This effect is more pronounced in the northern part of the domain (low y-values). It could also be seen that S2 dense has a higher concentration than S2 sparse and that S2 base has a higher concentration than S2 sparse at the right side of Fabriksgatan. When S2 dense and S2 base are compared, they seem to have roughly the same concentrations in that area (the area is mostly green). If compared to the tables in section 4.2.2, has S2 dense the highest concentrations for

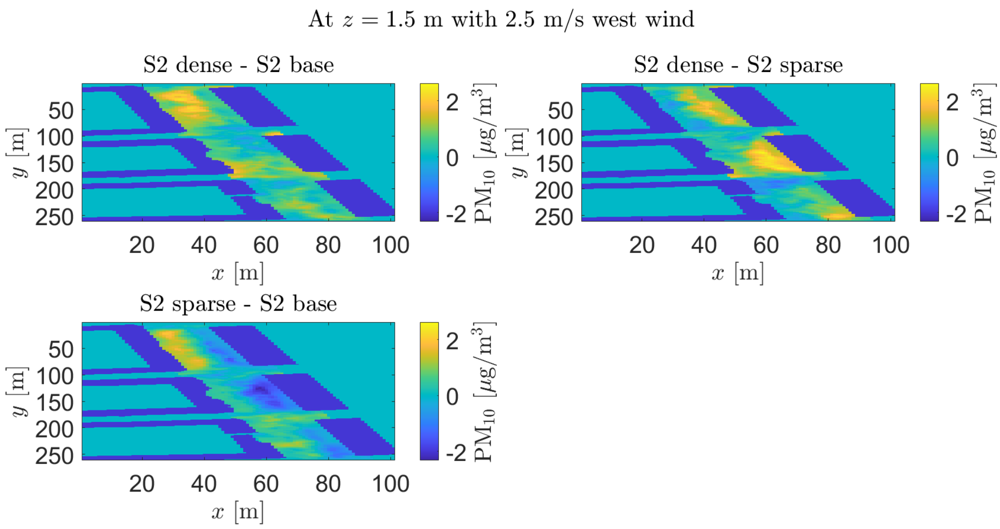

Figure 4.4: *Difference between concentration of PM_{10} (in $\mu g/m^3$) for S2 dense and S2 base, S2 dense and S2 sparse and S2 sparse and S2 base for $z = 1.5\,m$ and $2.5\,m/s$ west wind.*

all pollutants (except O_3), while S2 base and S2 sparse have roughly the same levels.

For S2 dense, both wind and concentration of PM_{10} (in $\mu g/m^3$) are visualised for $z = 10.5\,m$, which corresponds to inside the canopy of the row of trees. Figure 4.5 shows for $5.0\,m/s$ west wind and figure 4.6 shows for $5.0\,m/s$ east wind. It could be seen in both figures that in areas wind high concentration (yellow areas) the wind is directed upwards (arrows pointing up), while in areas with lower concentrations (blue areas), the wind is directed downwards (arrows pointing down). A reason for that the wind is pointed upwards where the concentrations is high is believed to be due to that when the wind reaches the buildings, the wind is forced upwards (and the pollution is gathered in those points).

The row of trees is located to the left (see figure 3.15). To see the effect of the row of trees, S2 base is used as comparison. Figure 4.7 shows concentration of PM_{10} (in $\mu g/m^3$) for $5.0\,m/s$ west wind (at $z = 10.5\,m$). By comparing this figure with figure 4.5, it could be seen that the concentration of PM_{10} is higher in the west side for the dense case, which could be because of less circulation due to the row of trees.

In all three figures (figure 4.5, figure 4.6 and figure 4.7), the pollution levels are higher on the same side that the wind is directed from (high levels on the west side for western wind and high levels on the east side for eastern wind).

Also here, the topography is taken into account, and the data is obtained in a similar way as described in section 4.2. This means that for figure 4.4, the data is obtained at the second level with values and for figure 4.5, figure 4.6 and figure 4.7, the data is obtained at the eleventh level with values. This was first believed to be the reason to that wind and concentration varies between the two sides of Fabriksgatan (since data from nearby points could be separated to different layers, depending on the terrain height), but when the data is visualised as a cross section instead, a similar pattern is obtained.

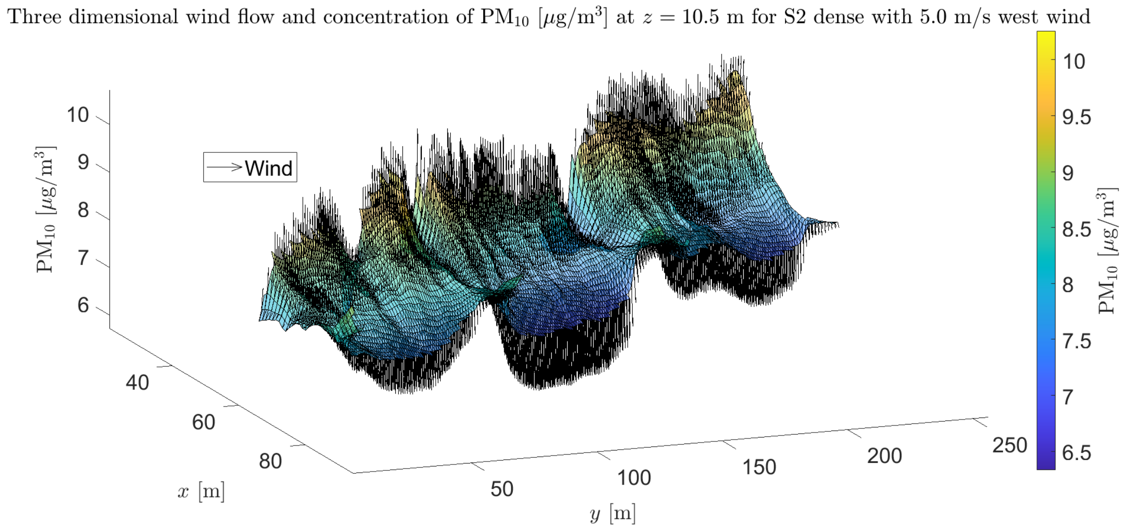

Figure 4.5: *Concentration of PM_{10} (in $\mu g/m^3$) at $z = 10.5\,m$ and three dimensional wind flow (represented by arrows) for S2 dense with $5.0\,m/s$ west wind.*

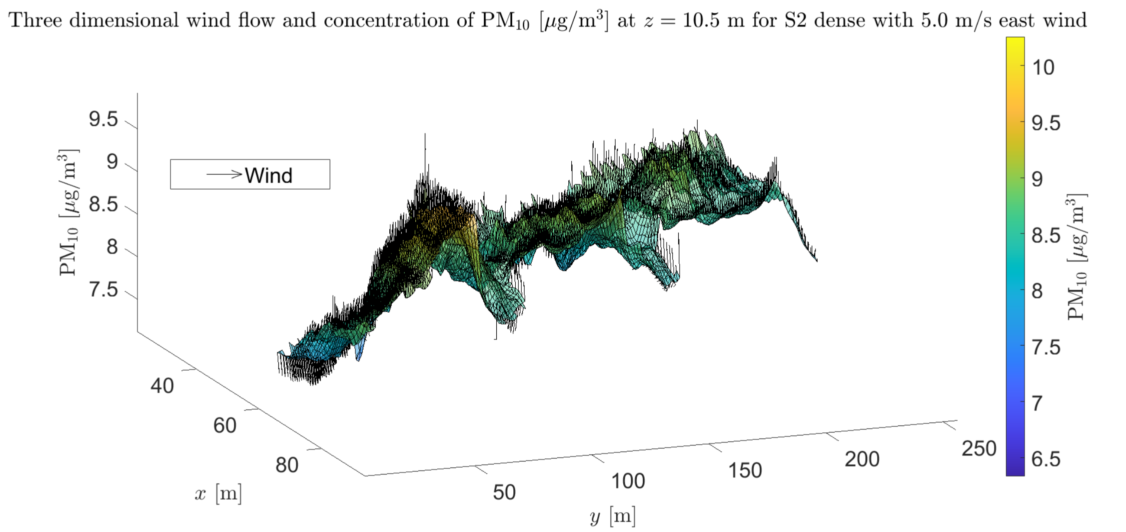

Figure 4.6: *Concentration of PM_{10} (in $\mu g/m^3$) at $z = 10.5\,m$ and three dimensional wind flow (represented by arrows) for S2 dense with $5.0\,m/s$ east wind.*

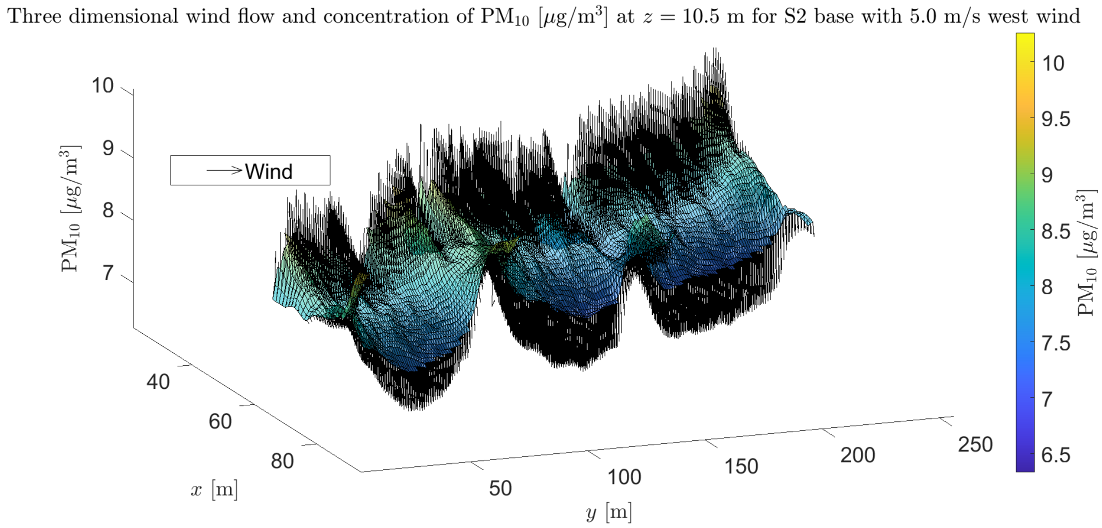

Figure 4.7: *Concentration of PM_{10} (in $\mu g/m^3$) at $z = 10.5\,m$ and three dimensional wind flow (represented by arrows) for S2 dense with $5.0\,m/s$ west wind.*

Chapter 5

Discussion and further developments

5.1 Simple model

Concentrations of NO, NO_2 and PM_{10} are highest in the S3 scenario. Concentration of O_3 is highest in the S1 scenario. S1 is also the scenario with the lowest concentrations of NO_2 and PM_{10}, and with almost the lowest concentration of NO and since there is a relationship between NO, NO_2 and O_3, this is not unexpected. Concentrations also do not vary much between the scenarios, especially for NO_2 and O_3.

A bit of the are close to the highway is included in the area of interest (see the red rectangle in for example figure 3.3), causing the concentrations of NO, NO_2 and PM_{10} to rise, but this is not the only reason for the high values. As mentioned in section 3.4, the emission and background data are just example values (and higher than the true values) and will not reflect the actual case for the simple model, just the relations.

5.2 Advanced model

The relative humidity is below 40% for all studied cases (see table 4.2). Thus well below 100%, meaning that cloud formation is avoided.

As seen in the tables in section 4.2.2, the relative concentrations are highest for all pollutants (except O_3) for scenario S0 and S5. These two scenarios have a narrower street canyon, which will decrease the circulation. S5 has higher relative concentrations than S0 for all pollutants except O_3. S5 has more homogeneous buildings, while they are more varied in S0, both in shape and height. This is believed to increase the circulation in S0, which is supported by Carpentieri and Robins (2015).

If only scenarios with the wider street (S1, S2, S3, S4 and S6) are studied, the highest concentrations are usually found in scenarios S2 and S3. The lowest concentrations are usually found in scenarios S1 and S6, and S4 is somewhere in between. Both S1 and S6 have point houses to the left of Fabriksgatan which increases the circulation. S6 has houses that forms a wall against the highway, but not S1, which not seem to affect the relative concentrations in a substantial way (at least not for the western wind that is studied). S2 and S3 have the same houses to the left of Fabriksgatan and both have houses that covers almost the full length of the right side of Fabriksgatan (more in S3 than in S2). This decreases the ability for circulation, which in turn impair the air quality. S4 has a more varied height distribution, but the lack of point houses is believed to put them in the middle.

For the vegetation scenarios, dense is often the scenario with the highest concentrations and base and sparse usually have the same concentrations. This is believed to be due to the consequence that a dense row of trees decreases the mixing with clean air. Point concentrations for different vegetation scenarios was also studied, but it is hard to draw conclusions from the tables with point concentrations since those vary substantially from point to point. But for point 1, 3 and 5 in the row of trees or to the left of the row of trees (at the bike- and walkway), the concentrations are often higher for dense than for base (see for example for S3 in table 4.14 and for S4 table 4.15) but not for all points always, see for example point 5 for S1 in table 4.12 and point 1 for S2 in table 4.13. But as mentioned, these are just point concentrations and the relative mean concentrations are more reliable when making comparisons.

For the wind configurations, it could be seen in table 4.17 that a high western wind has the lowest pollution levels, but that high eastern winds do not have as low levels (but the highest levels are obtained with a low western wind). In table 4.18, it could be seen that S3 has lower concentrations of PM_{10} than S2 for eastern wind. When S2 and S3 were compared for a 2.5 m/s west wind in table 4.6, S3 had higher levels than S2. Thus, the lower concentrations of S3 for eastern wind is not because of lower concentrations of S3 in general. For the point concentrations, it is mentioned in section 4.2.5 that point 3 is highest for a moderate (2.5 m/s) and a high (5.0 m/s) western wind for scenario S2 base and S2 dense. For a moderate (2.5 m/s) and a high (5.0 m/s) eastern wind, the concentration at point 2 is highest. Thus, the hypothesis is that for scenario S2, points to the west of Fabriksgatan have higher concentrations for western wind (point 3 is believed to have higher concentrations than the other point at the western side since that point lies closer to the emissions at the street) and points to the east of Fabriksgatan have higher concentrations for eastern wind. This is supported by the results in section 4.2.10. Point concentrations for the less confined street environment in S1 was studied for a moderate western wind (see table 4.12), and there have all points to the west (point 1, 3 and 5) lower concentrations than the points to the east (point 2 and 4). Scenario S3 has a more confined street environment than S2, and for S3 base (see table 4.14) with a moderate western wind, this also applies. But for a moderate eastern wind (see S3 base and dense in table 4.22), the concentrations are higher on the eastern side. This leads to the conclusion that the hypothesis that the concentration is higher on the side that the wind is blowing from only works for S2 (with moderate and high west and eastern wind) and S3 with moderate eastern wind. It could also be that it holds for eastern wind for all building scenarios, but since that only is supported by S2 and S3 (the only simulations run with eastern wind), it needs to be further investigated. This indicates that the preferable wind configurations differ from case to case. Which could be welcome, since the wind will vary from day to day. The wind is prescribed at the top of the domain, meaning that the wind at the surface could differ substantially from the top of the domain, especially within a complex environment such as the street canyon.

The environment is more open around the highway, causing the wind to transport the emissions from the highway. It could be seen in table 4.21 that S2 has higher pollution levels than S3 when the wind is directed from east to west. It was seen in table 4.6, that for western wind, has S3 higher levels than S2. This indicated that the blocking houses have an effect (which is also supported by table 4.18 where the concentration of PM_{10} is higher for S2 base and S2 dense than for S3 base and dense). Table 4.21 also indicates what has been discussed earlier, that vegetation scenario dense has higher concentration than vegetation scenario base.

The results from the emission scenarios do not contain any surprises. All scenarios with more traffic have higher levels of PM_{10} than today, which is normal since the PM_{10} emissions increase the same for 10% more traffic, independent of if the traffic increase contains electric vehicles or not. The levels of NO_2 are lower for scenarios with electric vehicles, which is as it should.

Pollution levels increase with green walls for scenario S3 base, see table 4.29. This indicates that green walls decrease the ventilation, supported by Abhijith et al. (2017).

When the ability of the dense row of trees to act as a shield was studied, concentration decreased on the leeward side for western wind but increased for eastern wind. The eastern wind was quite strong before the row and did then turn to a weak western wind. The western wind turned in one case and was enhanced in the second case (see table 4.32). This indicates that the row of trees could be used as a shield, but that it is important to study this in detail to not risk increasing the concentration behind the shield instead.

As mentioned in the last part of section 4.2.10, the concentration is higher at the same side that the wind is coming from in the cases visualised in figure 4.5, figure 4.6 and figure 4.7, which also is discussed earlier. This could seem contradicting since it would be intuitive if pollutants are accumulated at the eastern side for western wind (which is blowing from west to east). A reason for that this is not the case is that the wind is prescribed in the top of the domain, and there are many obstacles between the top of the domain and the surface within the street canyon, changing the wind flow. As could be seen in the figures, the wind (the black arrows) is mostly directed upwards or downwards, and not as much in the xy-plane.

It is interesting to see how the simulated values align with the measured values. Table 5.1 shows the mean value of NO, NO_2, O_3, PM_{10} and $PM_{2.5}$ the same day and time as the simulation is performed (28 June 2019, 10.00-12.00). Data for three measure stations are presented; Femman (at 30 m), Gårda (at 3 m) and Haga (at 3 m). Note that not all pollutants are measured at all stations. These values will be compared against the concentrations in scenario S0, which represents today. These values are presented as mean values for the focus area in table 5.2.

The values for NO and NO_2 are of the same order of magnitude as those for Gårda, and ten times larger than the values for Femman and Haga. The value for O_3 agree with the value for Femman (the only value for O_3). The value for PM_{10} lies

Table 5.1: *Values at measure station Femman, Gårda and Haga for NO, NO_2, O_3, PM_{10} and $PM_{2.5}$ 28 June 2019, 10.00-12.00. Data from SMHI (n.d.[a]).*

	NO [ppm]	NO_2 [ppm]	O_3 [ppm]	PM_{10} [µg/m^3]	$PM_{2.5}$ [µg/m^3]
Femman	0.00140	0.00449	0.02872	10.950	6.125
Gårda	0.01166	0.01200	-	15.300	-
Haga	0.00794	0.00818	-	-	-

Table 5.2: *Mean values for NO, NO_2, O_3, PM_{10} and $PM_{2.5}$ for scenario S0 (within the focus area) with* 2.5 m/s *west wind and at* $z = 1.5$ m.

	NO [ppm]	NO_2 [ppm]	O_3 [ppm]	PM_{10} [µg/m^3]	$PM_{2.5}$ [µg/m^3]
S0	0.017	0.014	0.031	12.077	3.490

between the values for Femman and Gårda and the value for $PM_{2.5}$ is a bit smaller than the value for Femman (the only value for $PM_{2.5}$). Even if the values do not align perfectly, they are somewhat aligned and the simulated values gives an idea of what the pollution levels will be in the different scenarios. And that is not the most important part of this project, it is more important to compare the scenarios with each other to see which scenarios that give the lowest (relative) levels of pollutants.

It is of interest to compare the simulated values with the guidelines, see table 2.1. In table 5.3, mean values for NO_2, O_3, PM_{10} and $PM_{2.5}$ are presented for the focus area at $z = 1.5$ m for S0, S1, S2, S3, S4, S5 and S6 for all vegetation scenarios (NO are excluded since it is not harmful for humans). Those values that are above the guidelines (the lowest value of the values from WHO and Swedish EPA will be used as the guideline) are marked in red and those that are below are green. The guidelines are given as a mixture of daily, hourly and 8-hour means but they will all be compared to the hourly mean obtained in the simulations (the simulations run as previously mentioned for two hours but only the last hour is used).

There are only two values that exceed the guidelines, NO_2 for S0 and S5. As mentioned above, the simulated values are not perfectly aligned with the actual values, which could make such comparisons as this one hard to make. The simulated value for NO_2 is actually larger than the measured one, which indicates that the actual values with different scenarios would be below the guidelines.

It is worth to mention that in the simulations, scenarios with the highest pollutant concentrations of NO, NO_2, PM_{10} and $PM_{2.5}$, have the lowest concentration of O_3. This is because of the chemical reactions between NO, NO_2 and O_3, which causes low levels of O_3 when the concentrations of NOx is high.

A possible reason that the green walls impaired air quality beyond decreased air flow, is that deposition is not yet fully implemented in PALM. Dry-deposition is turned on, but only for horizontal surfaces. One run is made with dry-deposition turned off to investigate any differences for scenario S2 dense and 2.5 m/s west wind. With dry-deposition on, the mean concentration of PM_{10} in the focus area is 10.461 µg/m^3, and 10.821 µg/m^3 with dry-deposition turned off. NO_2 is also tested to see if there are any differences between gases and aerosols. With dry-deposition on, the concentration of NO_2 is 0.0119 ppm in the focus area, and 0.0121 ppm with no

Table 5.3: *Mean values for NO_2, O_3, PM_{10} and $PM_{2.5}$ for scenario S0, S1, S2, S3, S4, S5 and S6 (within the focus area) with* 2.5 m/s *west wind and at* $z = 1.5$ m, *for all vegetation scenarios.*

	NO_2 [ppm]	O_3 [ppm]	PM_{10} [µg/m^3]	$PM_{2.5}$ [µg/m^3]
S0	0.014	0.031	12.077	3.490
S1 base	0.009	0.034	8.901	3.230
S1 dense	0.010	0.033	9.350	3.294
S1 sparse	0.009	0.034	8.884	3.229
S2 base	0.011	0.033	9.813	3.310
S2 dense	0.012	0.032	10.461	3.368
S2 sparse	0.011	0.033	9.847	3.306
S3 base	0.010	0.033	9.825	3.289
S3 dense	0.012	0.032	10.486	3.354
S3 sparse	0.011	0.033	10.121	3.325
S4 base	0.010	0.034	9.525	3.280
S4 dense	0.012	0.033	10.216	3.354
S4 sparse	0.010	0.033	9.697	3.295
S5	0.016	0.030	13.443	3.585
S6 base	0.010	0.034	9.263	3.265
S6 dense	0.010	0.033	9.388	3.284
S6 sparse	0.009	0.034	9.164	3.244

dry-deposition. For both NO_2 and PM_{10}, the mean concentration is higher without dry-deposition. Dry-deposition on all vegetation (and not only vegetation at the surface as in the chemistry module) is included in the aerosol module SALSA (PALM group, 2021g). A further development could be to include this module to study the effects of deposition, but this module is more computationally demanding.

One problem is that the proposed designs will take years to build, or even decades. Then, at least, the NOx concentrations will have decreased because of cleaner transportation. The traffic will also affect the wind flow, and this is neglected in PALM.

Even if vegetation sometimes has a negative impact on air quality, other benefits, such as for example carbon storage and regulation of humidity must be taken into account. Also, the positive social aspects of vegetation in cities must not be neglected. Vegetation could also be used as a noise barrier (Baldauf, 2017), which is another positive social aspect. Houses could of course also be used as noise barriers, for example the house to the right of Fabriksgatan in scenario S3, which forms a wall against the highway.

Different kinds of vegetation could be interesting to study in further research, for example study other leaf area densities to investigate porosity. Both for the green walls and also for the row of trees. Green roofs could be a natural development of green walls, even if they are inferior to green walls according to Abhijith et al. (2017). It could also be interesting to study other kind of vegetation, such as hedges. Wang, Gao, and Lv (2018) suggest that hedges could be used since they could be more effective in reducing concentrations and that they also are closer to the pollution sources, thereby decreasing the pollution even more. According to Santiago, Martilli, and Martin (2017), the benefits of deposition close to the source will be larger than the reduction of ventilation, if the vegetation is close to the source. Hedges could be located closer to the street and thereby closer to the source.

Baldauf (2017) suggest a mixture of vegetation, low bushes and high trees, to ensure a complete coverage, and also to prevent monocultures. This is an important ecological aspect, and such a mixture could be interesting to study as a barrier.

Another topic for further research could be to study a day with completely different weather conditions, for example a winter day when the risk of inversion is much higher. It is of interest to see if building and vegetation designs that are favourable during summer also are favourable during winter.

Chapter 6

Conclusions

The main conclusions will be listed in the following list as answers to the research questions stated in section 2.5, which where connected to the aim.

1. Small point houses are better for the air quality than larger houses.
2. A wide street canyon is better for the air quality than a narrow.
3. It is hard to determine how wind speed and direction affect the air quality, since a street canyon is such a complex environment. But for a rather confined street environment (scenario S2) and wind speeds of 2.5 m/s and over, concentrations are higher at the same side that the wind is coming from. This also holds for a confined street environment (scenario S3) and an eastern wind of 2.5 m/s. It needs to be further investigated with different wind directions for more scenarios before actual conclusions could be made.
4. Emissions scenarios with higher emissions of a pollutant gives higher concentrations of that pollutant.
5. Houses could be used as barriers to block emissions.
6. A row of trees could be used to shield out emissions at for example a bike- and walkway but increases the general pollution levels. A dense row of trees generally gives higher pollution concentrations than a sparse row of trees. The effect of deposition needs to be investigated further to see how a row of trees affect the pollution levels.
7. Green walls decrease the circulation and thus the benefits of deposition must be studied more, to evaluate the effect of green walls.

Bibliography

Abhijith, K. V., Prashant Kumar, John Gallagher, Aonghus McNabola, Richard Baldauf, Francesco Pilla, Brian Broderick, Silvana Di Sabatino, and Beatrice Pulvirenti (2017). "Air pollution abatement performances of green infrastructure in open road and built-up street canyon environments – A review". In: *Atmospheric Environment* 162, pp. 71–86. ISSN: 18732844. DOI: `10.1016/j.atmosenv.2017.05.014`.

Aristodemou, Elsa, Luz Maria Boganegra, Laetitia Mottet, Dimitrios Pavlidis, Achilleas Constantinou, Christopher Pain, Alan Robins, and Helen ApSimon (2018). "How tall buildings affect turbulent air flows and dispersion of pollution within a neighbourhood". In: *Environmental Pollution* 233, pp. 782–796. ISSN: 18736424. DOI: `10.1016/j.envpol.2017.10.041`.

Arneth, Almut, Nadine Unger, Markku Kulmala, and Meinrat O. Andreae (2009). "Clean the Air, Heat the Planet?" In: *Science* 326.5953, pp. 672–673. ISSN: 00368075. DOI: `10.1126/science.1181568`.

Baldauf, Richard (2017). "Roadside vegetation design characteristics that can improve local, near-road air quality". In: *Transportation Research Part D: Transport and Environment* 52, pp. 354–361. ISSN: 13619209. DOI: `10.1016/j.trd.2017.03.013`.

Buccolieri, Riccardo, Jose Luis Santiago, Esther Rivas, and Beatriz Sáanchez (2019). "Reprint of: Review on urban tree modelling in CFD simulations: Aerodynamic, deposition and thermal effects". In: *Urban Forestry and Urban Greening* 37.July 2018, pp. 56–64. ISSN: 16108167. DOI: `10.1016/j.ufug.2018.07.004`.

Cai, Mengfan, Zhongbao Xin, and Xinxiao Yu (2017). "Spatio-temporal variations in PM leaf deposition: A meta-analysis". In: *Environmental Pollution* 231, pp. 207–218. ISSN: 18736424. DOI: `10.1016/j.envpol.2017.07.105`.

Carpentieri, Matteo and Alan G. Robins (2015). "Influence of urban morphology on air flow over building arrays". In: *Journal of Wind Engineering and Industrial Aerodynamics* 145, pp. 61–74. ISSN: 01676105. DOI: `10.1016/j.jweia.2015.06.001`.

Cescatti, A. and B. Marcolla (2004). "Drag coefficient and turbulence intensity in conifer canopies". In: *Agricultural and Forest Meteorology* 121.3-4, pp. 197–206. ISSN: 01681923. DOI: `10.1016/j.agrformet.2003.08.028`.

Denby, B. R., I. Sundvor, C. Johansson, L. Pirjola, M. Ketzel, M. Norman, K. Kupiainen, M. Gustafsson, G. Blomqvist, and G. Omstedt (2013). "A coupled road dust and surface moisture model to predict non-exhaust road traffic induced particle emissions (NORTRIP). Part 1: Road dust loading and suspension modelling". In: *Atmospheric Environment* 77, pp. 283–300. ISSN: 13522310. DOI: 10.1016/j.atmosenv.2013.04.069.

ECMWF (n.d.). *L60 model level definitions*. URL: https://www.ecmwf.int/en/forecasts/documentation-and-support/60-model-levels.

Eljarrat, Ethel, Fei Li, M Jahangir Alam, Elisavet Stavropoulou, Ioannis Manisalidis, Agathangelos Stavropoulos, and Eugenia Bezirtzoglou (2020). "Environmental and Health Impacts of Air Pollution: A Review". In: *Frontiers in Public Health | www.frontiersin.org* 8, p. 14. DOI: 10.3389/fpubh.2020.00014.

European Commission (2010). *Air Pollution and Climate Change*. Tech. rep. Science for Environment Policy.

Fluid Mechanics 101 (Sept. 2020). *[CFD] Large Eddy Simulation (LES): An Introduction - YouTube*. URL: https://www.youtube.com/watch?v=r5vP45_6fB4.

Giardina, M. and P. Buffa (2018). "A new approach for modeling dry deposition velocity of particles". In: *Atmospheric Environment* 180.March, pp. 11–22. ISSN: 18732844. DOI: 10.1016/j.atmosenv.2018.02.038.

Göteborg Stad (n.d.). *Trafikmängder på olika gator*. URL: https://goteborg.se/wps/portal/start/gator-vagar-och-torg/gator-och-vagar/statistik-om-trafiken/trafikmangder-pa-olika.

Hassan, Asmaa Mohammed, Ashraf Abdel Fatah El Mokadem, Naglaa Ali Megahed, and Osama Mahmoud Abo Eleinen (2020). "Improving outdoor air quality based on building morphology: Numerical investigation". In: *Frontiers of Architectural Research* 9.2, pp. 319–334. ISSN: 20952635. DOI: 10.1016/j.foar.2020.01.001.

HBEFA (n.d.). *The Handbook Emission Factors for Road Transport*. URL: https://www.hbefa.net/e/index.html.

Hersbach, H., B. Bell, P. Berrisford, G. Biavati, A. Horányi, J. Muñoz Sabater, J. Nicolas, C. Peubey, R. Radu, I. Rozum, D. Schepers, A. Simmons, C. Soci, D. Dee, and J-N Thépaut (2018). *ERA5 hourly data on pressure levels from 1979 to present. Copernicus Climate Change Service (C3S) Climate Data Store (CDS).* URL: https://cds.climate.copernicus.eu/cdsapp#!/dataset/reanalysis-era5-pressure-levels?tab=form.

Inness, A, M Ades, A Agustí-Panareda, J Barré, A Benedictow, A Blechschmidt, J Dominguez, R Engelen, H Eskes, J Flemming, V Huijnen, L Jones, Z Kipling, S Massart, M Parrington, V-H Peuch, M Razinger, S Remy, M Schulz, and M Suttie (2019). *CAMS global reanalysis (EAC4). Copernicus Atmosphere Monitoring Service (CAMS) Atmosphere Data Store (ADS).* URL: https://ads.atmosphere.copernicus.eu/cdsapp#!/dataset/cams-global-reanalysis-eac4?tab=overview.

IRI/LDEO Climate Data Library (2021a). *NOAA NCEP-NCAR CDAS-1 MONTHLY Diagnostic 0-10_cm_down soil moisture*. URL: http://iridl.ldeo.columbia.edu/SOURCES/.NOAA/.NCEP-NCAR/.CDAS-1/.MONTHLY/.Diagnostic/.0-10_cm_down/.soil/.

— (2021b). *NOAA NCEP-NCAR CDAS-1 MONTHLY Diagnostic 0-10_cm_down temperature*. URL: http://iridl.ldeo.columbia.edu/SOURCES/.NOAA/.NCEP-NCAR/.CDAS-1/.MONTHLY/.Diagnostic/.0-10_cm_down/.temp/.

— (2021c). *NOAA NCEP-NCAR CDAS-1 MONTHLY Diagnostic 10-200_cm_down soil moisture*. URL: `http://iridl.ldeo.columbia.edu/SOURCES/.NOAA/.NCEP-NCAR/.CDAS-1/.MONTHLY/.Diagnostic/.10-200_cm_down/.soil/`.

— (2021d). *NOAA NCEP-NCAR CDAS-1 MONTHLY Diagnostic 10-200_cm_down temperature*. URL: `http://iridl.ldeo.columbia.edu/SOURCES/.NOAA/.NCEP-NCAR/.CDAS-1/.MONTHLY/.Diagnostic/.10-200_cm_down/.temp/`.

Jacobsson, Mark Z. (2012). *Air Pollution and Global Warming: History, Science, and Solutions*. Second edi. Cambridge: Cambridge University Press.

Janhäll, Sara (2015). "Review on urban vegetation and particle air pollution - Deposition and dispersion". In: *Atmospheric Environment* 105, pp. 130–137. ISSN: 18732844. DOI: `10.1016/j.atmosenv.2015.01.052`.

Johansson, Sara (2018). *The Influence of Land Cover on the Urban Energy Balance of Gothenburg*. Tech. rep., p. 46.

Karttunen, Sasu, Mona Kurppa, Mikko Auvinen, Antti Hellsten, and Leena Järvi (2020). "Large-eddy simulation of the optimal street-tree layout for pedestrian-level aerosol particle concentrations – A case study from a city-boulevard". In: *Atmospheric Environment: X* 6.March. ISSN: 25901621. DOI: `10.1016/j.aeaoa.2020.100073`.

Khan, Basit, Sabine Banzhaf, Edward Chan, Renate Forkel, Farah Kanani-Sühring, Klaus Ketelsen, Mona Kurppa, Björn Maronga, Matthias Mauder, Siegfried Raasch, Emmanuele Russo, Martijn Schaap, and Matthias Sühring (2020). "Development of an atmospheric chemistry model coupled to the PALM model system 6.0: Implementation and first applications". In: *Geoscientific Model Development Discussions* x, pp. 1–34. ISSN: 1991-959X. DOI: `10.5194/gmd-2020-286`.

Klingberg, Jenny, Janina Konarska, Fredrik Lindberg, Lars Johansson, and Sofia Thorsson (2017). "Mapping leaf area of urban greenery using aerial LiDAR and ground-based measurements in Gothenburg, Sweden". In: *Urban Forestry and Urban Greening* 26.October 2015, pp. 31–40. ISSN: 16108167. DOI: `10.1016/j.ufug.2017.05.011`.

Kurppa, Mona, Antti Hellsten, Mikko Auvinen, Siegfried Raasch, Timo Vesala, and Leena Järvi (2018). "Ventilation and air quality in city blocks using large-eddy simulation-urban planning perspective". In: *Atmosphere* 9.2, pp. 1–27. ISSN: 20734433. DOI: `10.3390/atmos9020065`.

Kurppa, Mona, Pontus Roldin, Jani Strömberg, Anna Balling, Sasu Karttunen, Heino Kuuluvainen, Jarkko V. Niemi, Liisa Pirjola, Topi Rönkkö, Hilkka Timonen, Antti Hellsten, and Leena Järvi (2020). "Sensitivity of spatial aerosol particle distributions to the boundary conditions in the PALM model system 6.0". In: *Geoscientific Model Development* 13.11, pp. 5663–5685. ISSN: 19919603. DOI: `10.5194/gmd-13-5663-2020`.

Lindberg, F, L Johansson, and S Thorsson (2013). *Träden i staden – användningen av LiDAR-data för att identifiera urban vegetation*. Tech. rep. University of Gothenburg, Department of Earth Sciences.

Maronga, B., M. Gryschka, R. Heinze, F. Hoffmann, F. Kanani-Sühring, M. Keck, K. Ketelsen, M. O. Letzel, M. Sühring, and S. Raasch (2015). "The Parallelized Large-Eddy Simulation Model (PALM) version 4.0 for atmospheric and oceanic flows: Model formulation, recent developments, and future perspectives". In: *Geo-*

scientific Model Development 8.8, pp. 2515–2551. ISSN: 19919603. DOI: 10.5194/gmd-8-2515-2015.

Maronga, Björn et al. (2020). "Overview of the PALM model system 6.0". In: *Geoscientific Model Development* 13.3, pp. 1335–1372. ISSN: 19919603. DOI: 10.5194/gmd-13-1335-2020.

Mistra Urban Futures (n.d.). *CityAirSim ska visa hur trafik, grönska och tätt byggande påverkar stadsluften | Mistra Urban Futures*. URL: https://www.mistraurbanfutures.org/sv/projekt/cityairsim-ska-visa-hur-trafik-gronska-och-tatt-byggande-paverkar-stadsluften.

National Weather Service (n.d.). *CLOUD DEVELOPMENT*. URL: https://www.weather.gov/source/zhu/ZHU_Training_Page/clouds/cloud_development/clouds.htm#CLOUD2.

Naturvårdsverket (Apr. 2020a). *Marknära ozon*. URL: https://www.naturvardsverket.se/Sa-mar-miljon/Klimat-och-luft/Luftfororeningar/Marknara-ozon/.

— (2020b). *Miljömålen Årlig uppföljning av Sveriges nationella miljömål 2020-Med fokus på statliga insatser*. Naturvårdsverket. ISBN: 9789162069193.

Nordling, Carl and Jonny Österman (2006). *Physics Handbook for Science and Engineering*. Lund: Studentlitteratur.

OpenStreetMap contributors (2021). *OpenStreetMap - Available under the Open Database License*. URL: https://www.openstreetmap.org/.

PALM group (2015). *PALM's Canopy Model*.

— (2021a). *PALM - Chemistry parameters*. URL: https://palm.muk.uni-hannover.de/trac/wiki/doc/app/chemistry_parameters.

— (2021b). *PALM - Land surface model*. URL: https://palm.muk.uni-hannover.de/trac/wiki/doc/tec/lsm.

— (2021c). *PALM - Land surface parameters*. URL: https://palm.muk.uni-hannover.de/trac/wiki/doc/app/land_surface_parameters.

— (2021d). *PALM - Nesting*. URL: https://palm.muk.uni-hannover.de/trac/wiki/doc/tec/nesting.

— (2021e). *PALM - Radiation model*. URL: https://palm.muk.uni-hannover.de/trac/wiki/doc/tec/radiation.

— (2021f). *PALM - Radiation parameters*. URL: https://palm.muk.uni-hannover.de/trac/wiki/doc/app/radiation_parameters.

— (2021g). *PALM - Salsa parameters*. URL: https://palm.muk.uni-hannover.de/trac/wiki/doc/app/salsa_parameters.

— (2021h). *PALM - Urban surface model*. URL: https://palm.muk.uni-hannover.de/trac/wiki/doc/tec/usm.

— (2021i). *PALM - Urban surface parameters*. URL: https://palm.muk.uni-hannover.de/trac/wiki/doc/app/urban_surface_parameters.

— (2021j). *PALM – Initialization parameters*. URL: https://palm.muk.uni-hannover.de/trac/wiki/doc/app/initialization_parameters.

Pérez, Gabriel, Julià Coma, Salvador Sol, and Luisa F. Cabeza (Feb. 2017). "Green facade for energy savings in buildings: The influence of leaf area index and facade orientation on the shadow effect". In: *Applied Energy* 187, pp. 424–437. ISSN: 0306-2619. DOI: 10.1016/J.APENERGY.2016.11.055.

Raasch, Siegfried and Michael Schröter (2001). "PALM - A large-eddy simulation model performing on massively parallel computers". In: *Meteorologische Zeitschrift* 10.5, pp. 363–372. ISSN: 09412948. DOI: 10.1127/0941-2948/2001/0010-0363.

Samad, A., U. Vogt, A. Panta, and D. Uprety (2020). "Vertical distribution of particulate matter, black carbon and ultra-fine particles in Stuttgart, Germany". In: *Atmospheric Pollution Research* 11.8, pp. 1441–1450. ISSN: 13091042. DOI: 10.1016/j.apr.2020.05.017.

Santiago, Jose Luis, Alberto Martilli, and Fernando Martin (2017). "On Dry Deposition Modelling of Atmospheric Pollutants on Vegetation at the Microscale: Application to the Impact of Street Vegetation on Air Quality". In: *Boundary-Layer Meteorology* 162.3, pp. 451–474. ISSN: 15731472. DOI: 10.1007/s10546-016-0210-5.

SCB (n.d.). *Fordonsstatistik.* URL: http://www.sverigeisiffror.scb.se/hitta-statistik/statistik-efter-amne/transporter-och-kommunikationer/vagtrafik/fordonsstatistik/.

SMHI (n.d.[a]). *Datavärdskap luft.* URL: https://datavardluft.smhi.se/portal/concentrations-in-air.

— (n.d.[b]). *Ladda ner meteorologiska observationer.* URL: https://www.smhi.se/data/meteorologi/ladda-ner-meteorologiska-observationer.

Sveriges geologiska undersökning (2020). *Glaciala finkorniga sediment.* URL: https://www.sgu.se/om-geologi/jord/fran-istid-till-nutid/isen-smalter/glaciala-finkorniga-sediment/.

— (2021). *Geokartan.* URL: https://apps.sgu.se/geokartan/.

Tritton, D. J. (1977). *Physical Fluid Dynamics.* 1st ed. Dordrecht: Springer.

UCAR Center for Science Education (2020). *How Weather Affects Air Quality.* URL: https://scied.ucar.edu/learning-zone/air-quality/how-weather-affects-air-quality.

Wang, Jia, He Gao, and Chundong Lv (2018). "Analysing the influence of different street vegetation on particulate matter dispersion using microscale simulations". In: *Desalination and Water Treatment* 110, pp. 319–327. ISSN: 19443986. DOI: 10.5004/dwt.2018.22333.

World Health Organization (2018). *Ambient (outdoor) air pollution.* URL: https://www.who.int/news-room/fact-sheets/detail/ambient-(outdoor)-air-quality-and-health.

— (2021a). *Ambient air pollution: Pollutants.* URL: https://www.who.int/airpollution/ambient/pollutants/en/.

— (2021b). *WHO global air quality guidelines : particulate matter (PM2.5 and PM10), ozone, nitrogen dioxide, surfur dioxide and carbon monoxide.* Tech. rep.

Appendix A

Conversion factors

In PALM's chemistry module is it important to have gases in ppm and particulate matter in kg/m^3. Values are sometimes given in mass per volume (for example kg/m^3 or µg/m^3) and therefore, a conversion to ppm will be presented.

The concentration of a gas $c_{\mathrm{g/m^3}}$ in mass per volume could be expressed as

$$c_{\mathrm{g/m^3}} = n_{gas} \cdot \frac{M}{V} \Leftrightarrow n_{gas} = \frac{c_{\mathrm{g/m^3}} V}{M}, \tag{A.1}$$

where n_{gas} [mol] is the amount of gas substance, M [g/mol] is the molar mass and V [m^3] the volume, meaning that the unit of c becomes g/m^3. The concentration in ppm, c_{ppm} is expressed as

$$c_{\mathrm{ppm}} = \frac{n_{gas}}{n_{tot}} \cdot 1 \cdot 10^6, \tag{A.2}$$

where n_{tot} is the amount of total substance. n_{tot} could be obtained using the ideal gas law (Nordling and Österman, 2006):

$$pV = n_{tot} RT \Leftrightarrow n_{tot} = \frac{pV}{RT}, \tag{A.3}$$

where p is the pressure, $R = 8.3145\,\mathrm{J/(mol \cdot K)}$ is the ideal gas constant and T the temperature. By using equation (A.1) and equation (A.3) in equation (A.2), a conversion between $c_{\mathrm{g/m^3}}$ and c_{ppm} is obtained:

$$c_{\mathrm{ppm}} = \frac{c_{\mathrm{g/m^3}} RT}{Mp} \cdot 1 \cdot 10^6.$$

If c is expressed in µg/m^3 instead of g/m^3, the factor $1 \cdot 10^6$ can be left out:

$$c_{\mathrm{ppm}} = \frac{c_{\mathrm{\mu g/m^3}} RT}{Mp}.$$

Emissions are sometimes given in g/s, while the input to the chemistry module should be in µmol/(m^2·day) for gases and kg/(m^2·day) for particulate matter. To go from g/s to kg/(m^2·day), the formula is

$$\text{Emissions}\left[\mathrm{kg/(m^2 \cdot day)}\right] = \text{Emissions}\,[\mathrm{g/s}] \cdot \frac{86400\mathrm{s/day}}{1000\mathrm{g/kg} \cdot A},$$

where A [m^2] is the area where the emissions occur (e.g. a road).

To go from g/s to µmol/(m^2·day) the formula is

$$\text{Emissions}\left[\text{µmol}/(\text{m}^2{\cdot}\text{day})\right] = \text{Emissions}\,[\text{g/s}] \cdot \frac{86400\text{s/day} \cdot 1 \cdot 10^{-6}\text{µg/g}}{M \cdot A},$$

where M [g/mol] is the molar mass.

MECHANICS AND MARITIME SCIENCES
CHALMERS UNIVERSITY OF TECHNOLOGY
Gothenburg, Sweden
www.chalmers.se

CHALMERS
UNIVERSITY OF TECHNOLOGY